

1 **Transported aerosols regulate the pre-monsoon ~~atmosphererainfall~~ over North-East**
2 **India: a WRF-Chem modelling study**

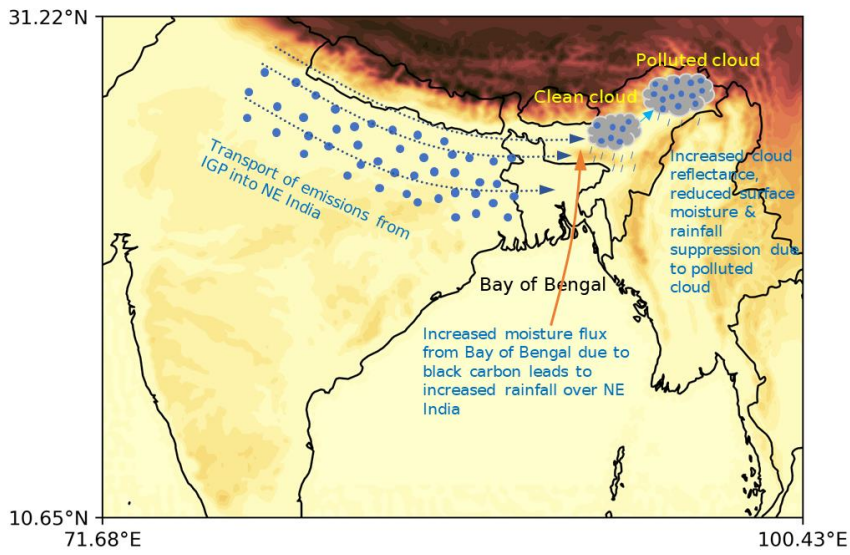
3 Neeldip Barman¹, Sharad Gokhale²

4 ¹Department of Civil Engineering, Indian Institute of Technology Guwahati, Guwahati, 781039, India

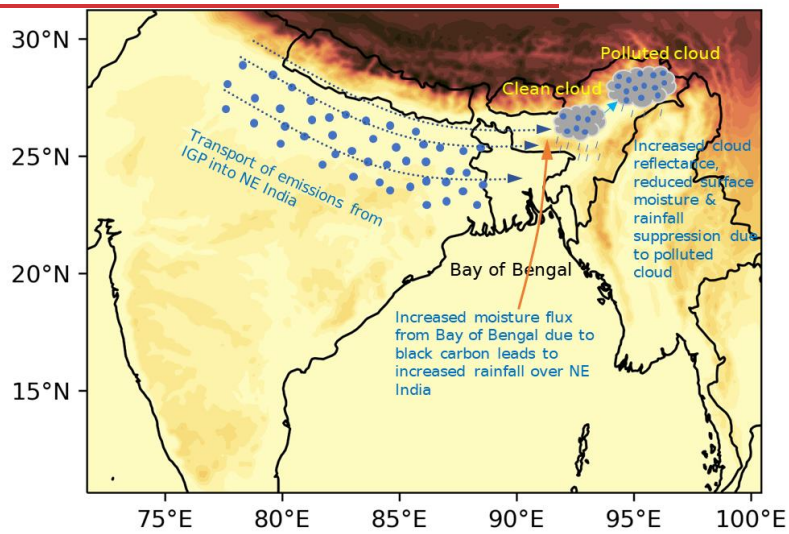
5 ²Department of Civil Engineering, Indian Institute of Technology Guwahati, Guwahati, 781039, India

6 *Correspondence to:* Sharad Gokhale (sharadbg@iitg.ac.in)

7 **Abstract.** The study differentiates and quantifies the impacts of aerosols emitted locally within North-East (NE)
8 India region and those transported from outside this region to ascertain whether local or transported aerosols are
9 more impactful in influencing this region's ~~atmosphererainfall~~ during the pre-monsoon season (March-April-
10 May). Due to the existence of a declining pre-monsoon rainfall trend in NE India, the study also quantified the
11 role of different aerosol effects ~~w.r.t~~on radiative forcing (RF) and rainfall. The study has been carried out using
12 the WRF-Chem model by comparing simulation scenarios where emissions were turned on and off within and
13 outside the NE region. The impact of all emissions as a whole and Black carbon (BC) specifically was studied.
14 Results show that aerosols transported primarily from the Indo-Gangetic Plain (IGP) were responsible for 93.98
15 % of the PM₁₀ mass over NE India's atmosphere and 64.18 % of near-surface PM₁₀ concentration. Transported
16 aerosols contributed >50 % of BC, organic carbon, sulfate, nitrate, ammonium and dust aerosol concentration and
17 hence a major contributor to air pollution. Hence, the aerosol effects were ~~observed to be~~ much greater with
18 transported aerosols. Indirect aerosol effect was found to be the major effect and more impactful with transported
19 aerosols that dominated both rainfall and RF, and suppressed rainfall significantly than the direct and semi-direct
20 effect. However, the increase in direct radiative effects with an increase in transported BC counteracted the rainfall
21 suppression caused by relevant processes of other aerosol effects. Thus, this study shows atmospheric transport
22 to be an important process for this region as transported emissions, specifically from IGP were also found to have
23 greater control over the region's rainfall. Thus, emission control policies implemented in IGP will reduce air
24 pollution as well as the climatic impacts of aerosols over the NE India region.



25



26

27 1 Introduction

28 Aerosols regulate the Earth's energy budget and hydrological cycle through scattering and absorption of solar
 29 radiation and acting as sites for the formation of cloud droplets, which leads to its varied effects, viz. direct, semi-
 30 direct and indirect effects (Mitchell, 1971; Rosenfeld, 2012; Menon et al., 2002). The effects differ spatially
 31 depending on the constituents of aerosols, their physical and chemical properties as well as the quantity. Among

32 these factors, atmospheric transport also plays an important role which extends the climatic impacts to the
33 transported region from the source region (Lee et al., 2022). The IGP is a global hotspot of diverse aerosols (Ojha
34 et al., 2020; Kumar et al., 2018) that impacts regional and global climate (Ramanathan et al., 2005; Tripathi et al.,
35 2005; Sarangi et al., 2015). Air masses transport aerosols from the IGP to nearby regions, which also impact air
36 quality (Bhat et al., 2022; Ojha et al., 2012). Bonasoni et al. (2010) showed that pollutants from the IGP follow
37 the southern slope of the Himalayas as a path into the Bay of Bengal and NE India and similar observations were
38 made by Gogoi et al. (2017). The condition becomes more critical in the pre-monsoon season when the westerlies
39 directly transport air pollutants from the IGP to NE India. Among the aerosols, BC is a high climate-influencing
40 aerosol component due to its strong absorption capability (Bond et al., 2013; Nenes et al., 2002; Koch and Del
41 Genio, 2010) and IGP is the largest source region of it in India (Rana et al., 2019). Several studies (Guha et al.,
42 2015; Sarkar et al., 2019; Chatterjee et al., 2010) found BC, among other aerosols measured at sites in NE India
43 to be transported from the IGP. Moreover, in the NE India region, an increase in BC emissions was observed
44 along with high BC concentrations near the surface level (Barman and Gokhale, 2019; Chaudhury et al., 2022;
45 Singh and Gokhale, 2021). Tiwari et al. (2016) observed maximum BC concentration during this season in this
46 region along with the highest surface RF. The region also observes the highest atmospheric heating and highest
47 aerosol optical depth with an increasing trend during this period (Nair et al., 2017; Dahutia et al., 2018; Dahutia
48 et al., 2019; Gogoi et al., 2017; Pathak et al., 2010; Pathak et al., 2016). The presence of high aerosol loading
49 along with high atmospheric heating is likely to have varied aerosol effects over the region and may also have an
50 important role to play with the rainfall. Mondal et al. (2018) showed a decreasing trend of pre-monsoon rainfall
51 in this biodiversity hotspot region. Few modelling studies (Kant et al., 2021; Kedia et al., 2016; Kedia et al., 2019)
52 are available that studied the aerosol effect on rainfall over India. However, only Soni et al. (2017) and Barman
53 and Gokhale (2022) studied the BC effect on pre-monsoon rainfall in this region but without the inclusion of
54 aerosol indirect effect. Both studies found BC to increase total rainfall but Barman and Gokhale (2022) also found
55 semi-direct effect to be a rainfall suppression mechanism by evaporating clouds between 1 to 2 km above ground
56 level.

57 However, a few questions remained to be answered. How much is the contribution of transported aerosols
58 to air pollution and climatic effects compared to those emitted within NE India region? What is the role of different
59 aerosol effects on the rainfall mechanisms? Thus, this study was carried out with the following objectives (a)
60 Compare the contributions of local and transported aerosols to air pollution and different climatic effects over NE
61 India (b) Quantify the role of different aerosol effects on the climatic effects (c) Investigate the role of BC emitted
62 within NE India and transported BC in such climatic effects. Here, transported aerosols include the transported
63 primary aerosols emitted from outside NE India as well as the secondary aerosols formed from the transported
64 emissions. Same goes for local emissions. Through qualitative and quantitative comparison of the impacts of local
65 and transported aerosols, the study tries to find the source region of aerosols that has a greater impact on the
66 atmosphere over NE India during the pre-monsoon season. Since observational studies cannot distinguish between
67 the local and transported aerosols impacts, the study was carried out with numerical modelling. The effect of
68 transported aerosols on different regions of the world has been studied (Krishnamohan et al., 2021; Wang et al.,
69 2020; Bagtasa et al., 2019) but none of them covered the IGP and its impact on the nearby region.

70 2 Methods

71 The study used the WRF-Chem v4.2.1 model (Grell et al., 2005). The model configuration, modelling domain,
 72 model inputs and simulation period is similar to the one used in Barman and Gokhale (2022), and details regarding
 73 the same is provided in that study. Details regarding physical and chemical parametrization schemes and as well
 74 the emissions are provided in Table 1.

75 Table 1: Details of physical parametrizations, chemical parametrizations and emissions

Physical parametrizations	
Planetary boundary layer	MYNN3 (Nakanishi and Niino, 2006)
Radiation	RRTMG (Iacono et al., 2008)
Land surface model	NOAH (Tewari et al., 2004)
Cumulus scheme	Grell-Freitas (Grell and Freitas, 2014)
Microphysics	Morrison (Morrison et al., 2009)
Meteorology initial and boundary conditions	ERA5 (Hersbach et al., 2020)
Chemical parametrizations and emissions	
Chemistry scheme	MOZART (Emmons et al., 2010)
Aerosol scheme	MOSAIC (Zaveri et al., 2008)
Chemistry initial and boundary conditions	CAM-Chem (Lamarque et al., 2012)
Anthropogenic emissions	CAMS emission inventory (Granier et al., 2019)
Fire emissions	FINN (Wiedinmyer et al., 2010)
Dust emissions	Online model (Zhao et al., 2010)
Biogenic emissions	MEGAN v2.04 (Guenther et al., 2006)

Formatted: Font: 10 pt, Not Italic, Font color: Auto, Complex Script Font: 10 pt, Not Italic

Formatted: Font: 10 pt, Complex Script Font: 10 pt

Formatted: Caption, Keep with next

Formatted: Font: Bold, Complex Script Font: Bold

Formatted Table

Formatted: Font: Bold, Complex Script Font: Bold

76
 77 The model was run at 10 km grid size for a duration of 13 days from 7-19 April 2018, out of which a 3-
 78 day period from 7-9 April 2018 was discarded as spin-up and outputs from 10-19 April 2018 were used for
 79 analysis. The period represents the mid of pre-monsoon season. Also, April 2018 was Indian Ocean Dipole and
 80 ENSO neutral period and hence suitable for study of aerosol effects. The model domain is shown in Fig. 1(a)
 81 which extends from 10.65° N to 31.22° N and 71.68° E to 100.43° E, and the NE India is the part of India within
 82 the region bounded by the blue box. The region within the box is bounded by 22° N and 29° N latitudes and 89°
 83 E and 97° E longitudes. The climatic situation during the study period was also described in Barman and Gokhale
 84 (2022). The near surface wind flow was from the Bay of Bengal towards NE India, which gradually changed to
 85 westerly wind flow carrying aerosols from IGP- towards NE India. Hence the domain was selected by keeping the
 86 NE India region near the upper-right corner of the domain. Descriptions of the simulations are provided in Table
 87 2+.

Formatted: Indent: First line: 1.27 cm

88 Table 2: Description of simulations

	Simulation name	Description of simulations
1.	NOR-I	Baseline simulation with all aerosol effects
2.	NOFEED-I	Same as NOR-I but with aerosol radiative effects turned off
3.	NOCHEM	Simulation with no atmospheric chemistry and aerosol effects
4.	No_EMISS_NE	Same as NOR-I but with emissions turned on only outside NE India

5.	Only_EMISS_NE	Same as NOR-I but with emissions turned on only within NE India
6.	No_EMISS_NE_4SO ₂	Same as No_EMISS_NE but with 4×SO ₂ emissions
7.	No_EMISS_NE_0.25SO ₂	Same as No_EMISS_NE but with 0.25×SO ₂ emissions
8.	No_EMISS_NE_NOFEED	Same as No_EMISS_NE but with aerosol radiative effects turned off
9.	Only_EMISS_NE_NOFEED	Same as Only_EMISS_NE but with aerosol radiative effects turned off
10.	No_NE_BCI	Same as NOR-I but with BC emissions turned on only outside NE India
11.	Only_NE_BCI	Same as NOR-I but with BC emissions turned on only within NE India
12.	4NOR-I	Same as NOR-I but with 4×BC emissions
13.	No_BC_ABS	Same as NOR-I but with BC absorption disabled
14.	NOR	Baseline simulation with only direct and semi-direct effect
15.	2NOR	Same as NOR but with 2×BC emissions
16.	No_NE_BC	Same as NOR but with BC emissions within NE India region turned off
17.	No_NE_2×BC	Same as No_NE_BC but with 2×BC emissions outside NE India
18.	Only_NE_BC	Same as NOR but with BC emissions turned off outside NE India
19.	Only_NE_2×BC	Same as Only_NE_BC but with 2×BC emissions inside NE India
20.	NOFEED	Same as NOR but with aerosol radiative effects off

89

90 All the simulations were conducted with the MOZART-MOSAIC ~~chemistry~~ scheme, except simulation 3, which
91 was purely a meteorology simulation and did not include any atmospheric chemistry and aerosol effects.
92 Moreover, simulations 1 to 13 (except 3), were conducted with the version of MOZART-MOSAIC scheme which
93 also supports indirect aerosol effect by coupling with the Morrison microphysics scheme along with direct and
94 semi-direct effect, while simulations 14 to 20 did not include indirect effect. The NOR simulation ~~which was used~~
95 in Barman and Gokhale (2022), ~~wasis~~ also used in this study. NOR-I is also the baseline simulation run with the
96 same baseline emissions for the study period as NOR, but also includes indirect aerosol effect. No_EMISS_NE
97 had all emissions (biogenic, anthropogenic and dust) disabled within the region bounded by 22° N and 29° N
98 latitudes and 89° E and 97° E longitudes, shown by the blue box in Figure 1(a) while No_NE_BC and No_NE_BCI
99 only had BC emissions disabled within the same region. Only_EMISS_NE had all emissions disabled outside of
100 the above region along with boundary conditions for all chemical species modified to zero to nullify the transport
101 of emissions from outside the domain and similarly, Only_NE_BC and Only_NE_BCI had BC emissions disabled
102 outside the NE India region with boundary conditions for BC modified to zero. Remaining simulations can be
103 understood from Table 2 and their applications ~~are is better~~ understood from the results and discussion in Sect 3.

104 As per Ghan et al. (2012) and Bauer and Menon (2012), the total aerosol effect is the algebraic sum of
105 direct, indirect and semi-direct effects. Similar approaches were used by Yang et al. (2011). Thus,

106
$$\text{NOR-I} - \text{NOCHEM} = \text{Total aerosol effect} = \text{Direct} + \text{Semi-direct} + \text{Indirect}, \quad (1)$$

107 Both NOFEED-I and NOR-I includes indirect effect but NOFEED-I does not include aerosol radiative effects.
108 Thus,

109
$$\text{NOR-I} - \text{NOFEED-I} = \text{Direct} + \text{Semi-direct effect}, \quad (2)$$

110 Also, since NOFEED-I includes only indirect effect,

111 NOFEED-I – NOCHEM = Indirect effect, (3)

112 Similar approaches were used by Wang et al. (2015).

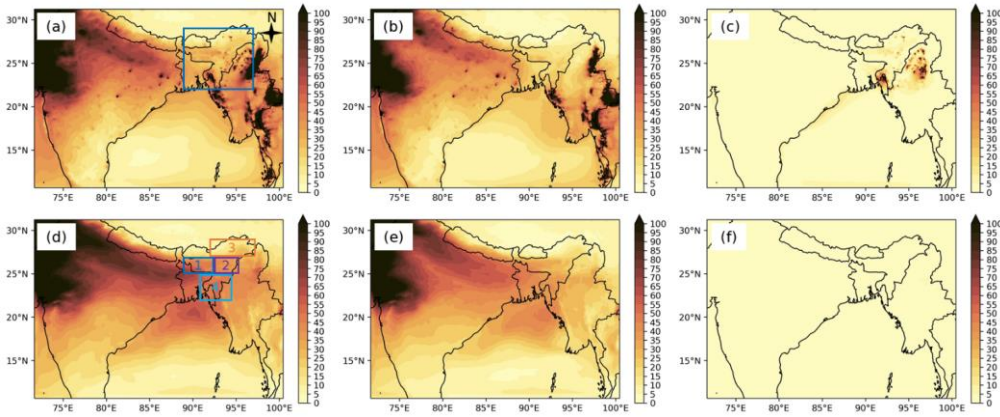
113 ~~No_EMITT_NE had all emissions (biogenic, anthropogenic and dust) disabled within the NE India region~~
114 ~~bounded by 22° N and 29° N latitudes and 89° E and 97° E longitudes, shown by the blue box in Fig. 1(a).~~
115 ~~Similarly, Only_EMITT_NE had all emissions disabled outside of the above region along with boundary~~
116 ~~conditions for all chemical species modified to zero to nullify the transport of emissions from outside the domain.~~
117 ~~Simulations 14 to 20 were specifically used to understand the contribution of local and transported BC emissions~~
118 ~~as well the response of emission increase on radiative heating, atmospheric dynamics and moisture without the~~
119 ~~interference of indirect aerosol effect.~~

120 The NOR simulation utilised in this study was evaluated in Barman and Gokhale (2022). Moreover,
121 meteorological evaluation of NOR-I w.r.t wind direction, wind speed, temperature and humidity was carried out
122 against surface station datasets (<https://mesonet.agron.iastate.edu/sites/locate.php>) at Guwahati (26.10 °N, 91.58
123 °E), Kolkata (22.65 °N, 88.45 °E), Bangalore (13.20 °N, 77.70 °E), Patna (25.59 °N, 85.08 °E), Delhi (28.56 °N,
124 77.11 °E) and Mumbai (19.10 °N, 72.86 °E). Simulated rainfall was evaluated against the Indian Meteorological
125 Department (IMD) rainfall dataset of Pai et al. (2014)
126 (https://www.imdpune.gov.in/Clim_Pred_LRF_New/Gridded_Data_Download.html). Index of agreement (IOA),
127 root mean square error (RMSE) and mean error (ME) were used as statistical parameters. As per the criteria of
128 Emery et al. (2001), the NOR-I simulation underpredicted temperature but showed good performance with wind
129 speed and wind direction but had large RMSE with wind direction, similar to the NOR simulation. Performance
130 statistics are provided in Table S1. Moreover, NOR and NOR-I simulated chemical species (BC, organic carbon,
131 dust and sulfate aerosol) were compared against the MERRA2 dataset
132 (https://disc.gsfc.nasa.gov/datasets/M2T1NXAER_5.12.4/summary) at the above locations. Performance
133 statistics are shown in Table S2. NOR gave a much better estimation of all the chemical species at all locations.
134 ~~Moreover, the predicted chemical species of nitric oxide (NO), nitrogen dioxide (NO₂), sulfur dioxide (SO₂),~~
135 ~~PM_{2.5} and PM₁₀ were compared against in-situ observations at Delhi (28.56 °N, 77.11 °E), Kanpur (26.57 °N,~~
136 ~~80.32 °E), Patna (25.61 °N, 85.13 °E) and Siliguri (26.69 °N, 88.41 °E), obtained from Central Pollution Control~~
137 ~~Board, India (<https://app.cpcbcr.com/ccr/#/caaqm-dashboard-all/caaqm-landing/caaqm-data-availability>). These~~
138 ~~locations are located along the IGP. Performance statistics are given in Table S3. The performance statistics were~~
139 ~~better with both particulate matter than gaseous species. Comparatively the performance was better with~~
140 ~~MERRA2. The relatively lower performance with in-situ comparison may be due to the grid size as in-situ~~
141 ~~observations are affected by local emission sources as well the deficiencies in emission inventory. However, the~~
142 inclusion of all aerosol effects greatly improved simulated rainfall performance with NE India regional average
143 IOA: 0.52, ME: 3.72 mm day⁻¹, RMSE: 13.55 mm day⁻¹ compared to only considering direct + semi-direct effect
144 (IOA: 0.40, ME: 9.22 mm day⁻¹, RMSE: 21.26 mm day⁻¹) in Barman and Gokhale (2022). The improvement in
145 performance and decrease in ME show that indirect effect played a major role during this period in controlling
146 and suppressing rainfall.

147 **3 Results and discussion**

Formatted: No underline, Font color: Auto

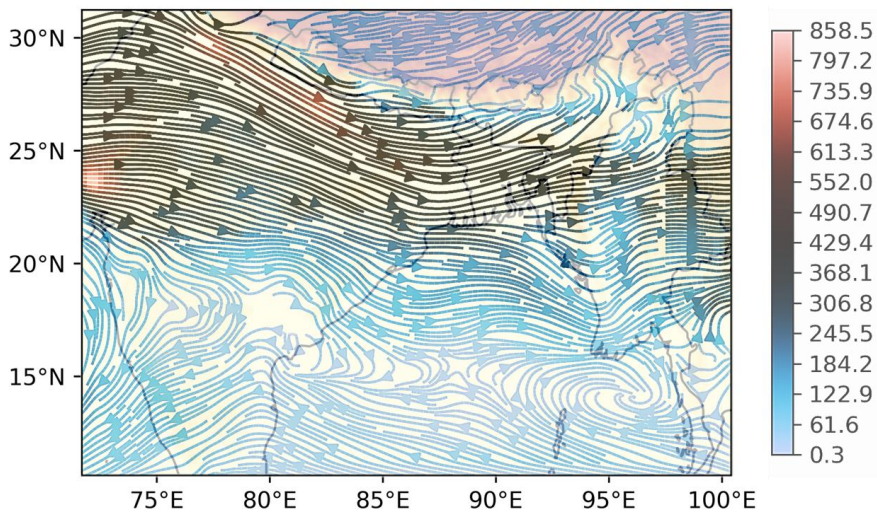
148 **3.1 PM₁₀ spatial and vertical atmospheric distribution**



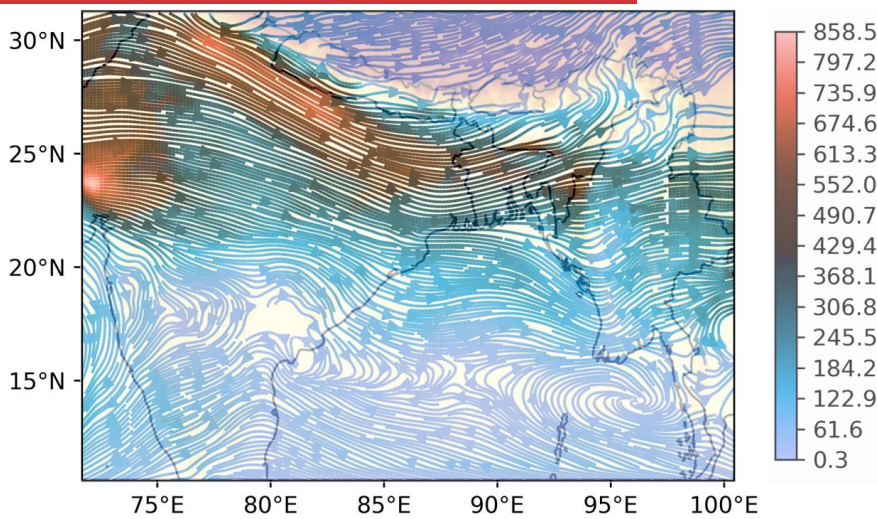
149
150 Figure 1: Spatial distribution of PM₁₀ concentration ($\mu\text{g m}^{-3}$) in NOR-I, (a, d), No_EMISS_NE (b, e) and
151 Only_EMISS_NE (c, f). Upper row shows distribution at model level 0 (near surface) and the lower row at model
152 level 15

153 Figure 1 shows the time-averaged spatial distribution of PM₁₀ concentration. The NE India region was divided
154 into four regions based on the proximity from the IGP, shown in Fig. 1(d). Region 1 and region 2 fall along the
155 Brahmaputra River Valley, with region 1 being closest to IGP. Region 3 is mostly a mountainous region and 4
156 Region 4 is the southern region closer to the Bay of Bengal. The spatial distribution of geopotential heights of
157 model level 0 and 15 are shown in Fig. S1, while region-wise (Fig. 1(d)) concentration values within NE India at
158 the two atmospheric heights are shown in Table S34. PM₁₀ concentration contours shown in Fig. 1(a), 1(b), 1(d)
159 and 1(e), emanating from IGP and spreading into NE India indicated the transport of aerosols from IGP into NE
160 India. The similarity of these spatial distributions of No_EMISS_NE to the baseline scenario, NOR-I, especially
161 within NE India region inferred that most of the aerosol mass within NE India was contributed by transported
162 aerosols, while PM₁₀ emitted or formed over NE India remained mainly confined within the region as shown in
163 Fig. 1(c), possibly due to the mountainous terrain, as also described in Kundu et al. (2018). The transport of PM₁₀
164 can also be seen from Fig. 2, in which the streamline's arrow from IGP to NE India show the transport of air-mass
165 and the colour of the streamlines show the PM₁₀ mass flux in $\mu\text{g m}^{-2} \text{s}^{-1}$. The flux was higher over IGP. The
166 transport of PM₁₀ can also be seen from Fig. 2, in which the streamlines from IGP to NE India show the transport
167 of air-mass and the colour of the streamlines show the PM₁₀ mass flux in $\mu\text{g m}^{-2} \text{s}^{-1}$. The flux is higher over IGP.

168



169



170

171

172 Figure 2: Streamlines showing transport of air-mass from IGP to NE India and PM₁₀ mass flux ($\mu\text{g m}^{-2} \text{s}^{-1}$) at 1300
 173 m above terrain.

174 Figure 2: Streamlines showing transport of air-mass from IGP to NE India and PM₁₀ mass flux at 1300 m

Formatted: Font: 10 pt, Complex Script Font: 10 pt

Formatted: Font: 10 pt, Complex Script Font: 10 pt

Formatted: Font: 10 pt, Complex Script Font: 10 pt

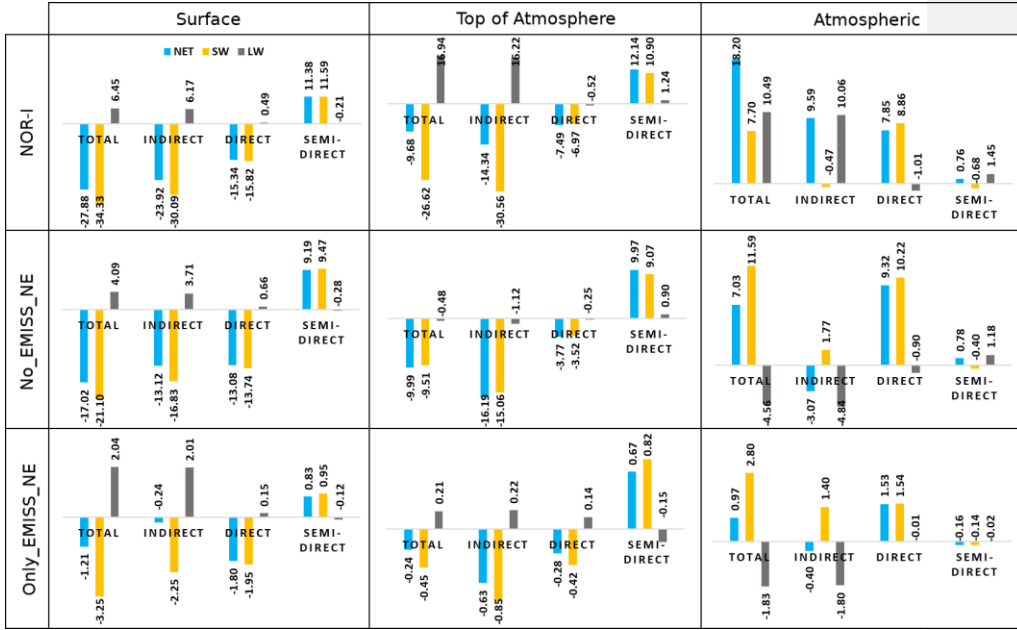
Formatted: Font: 10 pt, Complex Script Font: 10 pt

175 Both near the surface and at higher atmosphere (level 15), No_EMISS_NE showed a higher regional average
176 concentration (surface: $14.46 \mu\text{g m}^{-3}$, higher atmosphere: $24.43 \mu\text{g m}^{-3}$) which was closer to the baseline scenario
177 of NOR-I (surface: $27.43 \mu\text{g m}^{-3}$, higher atmosphere: $34.13 \mu\text{g m}^{-3}$) compared to the local emission scenario of
178 Only_EMISS_NE (surface: $8.07 \mu\text{g m}^{-3}$, higher atmosphere: $0.98 \mu\text{g m}^{-3}$). Thus, transported aerosols contributed
179 higher PM_{10} concentration (64.18 %) than local emission and contribution from local emissions were negligible
180 at higher atmosphere, as also seen in Fig. 1(f) and 96.14 % of it was contributed by transported aerosols. The
181 higher concentration at higher atmosphere was due to transported aerosols developing an elevated PM_{10} profile
182 (Fig. S2) having maximum concentration near 2000 m and which shows much greater similarity with the baseline
183 scenario. The long range transport and strong convective active during this season is responsible for the elevated
184 profile (Pathak et al., (2016)). Hence, transported aerosols contributed to bulk of the aerosols over NE India
185 throughout the atmospheric column (93.98 %) indicated by the column integrated PM_{10} mass of 313.97 g m^{-2}
186 (No_EMISS_NE) and 20.08 g m^{-2} (Only_EMISS_NE). NOR-I had column integrated PM_{10} mass of 466.63 g m^{-2} .
187 Further analysis indicated that transported aerosols accounted for >50 % of BC, organic carbon, sulfate, nitrate,
188 ammonium and dust aerosol mass over NE India's atmosphere as the column integrated mass for these species in
189 No_EMISS_NE were 4.55, 19.59, 51.66, 2.20, 13.74 and 207.82 g m^{-2} , respectively, while it was 0.94, 6.51, 1.79,
190 0.12, 0.56 and 6.60 g m^{-2} , respectively in Only_EMISS_NE. The spatial distribution of column integrated mass
191 of these species can be seen in Figures S3, S4, S5, S6, S7 and S8.—Regions 1, being in close proximity to IGP, as
192 seen in Fig. 1(c),—~~received~~, received maximum near surface aerosol mass (73.70 %) from transported aerosols,
193 compared to the other regions, followed by region 2 (66.86 %), 3 (60.48 %) and 4 (57.43 %). However, even
194 though No_EMISS_NE and Only_EMISS_NE is the bifurcation of NOR-I into two separate emission regions,
195 the sum of No_EMISS_NE and Only_EMISS_NE column integrated mass as well as concentrations didn't equate
196 to NOR-I values and is always less than it. This indicated formation of extra aerosol mass due to interaction of
197 emissions of the two regions.

198 3.2 Aerosol effects of local and transported aerosols on radiative forcing

199 RF due to different aerosol effects was estimated based on the methodology described in Sect. 2. Further details
200 regarding its estimation are provided in the supplementary.

201 The baseline scenario indicated that direct and indirect aerosol effects caused net (NET) surface and top
202 of the atmosphere (TOA) dimming while causing atmospheric heating, as seen in Fig. 3. This is due to the presence
203 of aerosols that scatter and absorb solar radiation, reducing it at the surface while increasing it at the top of the
204 atmosphere as well as causing atmospheric heating. Net direct surface, TOA and atmospheric RF were -15.34 , $-$
205 7.49 and 7.85 W m^{-2} and was mainly contributed by short-wave (SW) radiation. Indirect effect had the same effect
206 on solar radiation as the direct effect and was due to the formation of numerous smaller cloud droplets which has
207 better reflectivity to solar radiation, also known as the 1st indirect effect or Twomey effect (Twomey, 1977), and
208 However, positive atmospheric RF (18.20 W m^{-2}) causing atmospheric heating (10.06 W m^{-2}) was mainly caused
209 by long-wave (LW) radiation (16.22 W m^{-2}) at the TOA contributed by indirect effect. This was due to greater
210 cloud cover (Fig. S93) at 8 – 10 km which is not seen in the other two scenarios. The indirect effect also caused
211 warming at the surface (6.17 W m^{-2}), as its contributed to greater cloud cover (Nandan et al., 2022) and
212 causedcausing heating of the surface through LW radiation. The total net surface RF was -27.88 W m^{-2} out of
213 which -23.92 W m^{-2} or 85.80% was contributed



214

215 Figure 23: NE India regional average RF ($W m^{-2}$) due to different aerosol effects at NET, SW and LW wavelengths
 216 in different emission scenarios

217 by indirect forcing. Indirect SW forcing ($-30.08 W m^{-2}$) was almost twice the direct SW forcing ($-15.82 W m^{-2}$),
 218 while semi-direct SW forcing ($+11.58 W m^{-2}$) was $\sim 75\%$ of the direct forcing. Semi-direct effect showed positive
 219 surface RF due to cloud cover reduction. Thus, atmospheric heating and the subsequent evaporation of clouds
 220 compensated to a large extent the reduction in solar radiation due to aerosols. The atmospheric RF ($0.76 W m^{-2}$)
 221 due to semi-direct effect was due to LW radiation, which may be due to increased solar radiation at the surface,
 222 which released the heat into the atmosphere in the form of LW radiation. However, this value was very small. The
 223 indirect RF contributed most to the total surface, TOA and atmospheric RF at both SW and LW wavelengths and
 224 hence was found to be the dominant aerosol effect affecting radiation over NE India.

225 Quantitatively, No_EMISS_NE provided RF values (surface: $-17.02 W m^{-2}$, TOA: $-9.99 W m^{-2}$ and
 226 atmospheric RF: $7.03 W m^{-2}$) that were much similar and closer to the baseline scenario (surface: $-27.88 W m^{-2}$,
 227 TOA: $-9.68 W m^{-2}$ and atmospheric RF: $18.20 W m^{-2}$) than Only_EMISS_NE (surface: $-1.21 W m^{-2}$, TOA: -0.24
 228 $W m^{-2}$ and atmospheric RF: $0.97 W m^{-2}$). Consequently, the No_EMISS_NE net indirect, direct and semi-direct
 229 surface RF values of -13.12 , -13.08 and $9.19 W m^{-2}$ were significantly larger than the corresponding
 230 Only_EMISS_NE RF values of -0.24 , -1.80 and $0.83 W m^{-2}$. A similar conclusion could be inferred at TOA also.
 231 Hence transported aerosols were primarily responsible for all the different aerosol effects on radiation over NE
 232 India as a greater amount of aerosol mass was contributed by it. Moreover, No_EMISS_NE net direct atmospheric
 233 RF ($9.32 W m^{-2}$) was found to be even higher than the baseline scenario ($7.85 W m^{-2}$). This indicated that the NE
 234 India region contained more scattering aerosols while transported aerosols contained more absorbing aerosols as

235 the difference in the direct atmospheric RF is mainly driven by changes in the TOA RF (-7.49 vs. -3.77 W m⁻²)
 236 than surface RF (-15.34 vs. -13.08 W m⁻²). Region 1 had the highest direct and semi-direct net surface RF of -
 237 20.41 W m⁻² and 19.20 W m⁻², respectively due to its close proximity to IGP.

238 3.3 Aerosol effects of local and transported aerosols on rainfall

239 Table 23: Changes in rainfall due to different aerosol effects in different scenarios (mm)

	Total aerosol effect	Direct + semi-direct	Indirect
NOR-I	-275.13	-17.04	-258.09
No_EMISS_NE	-73.06	-23.95	-49.11
Only_EMISS_NE	-24.45	-8.42	-16.04

	Total aerosol effect	Direct + semi-direct	Indirect
NOR-I	-275.13	-17.04	-258.09
No_EMISS_NE	-73.06	-23.95	-49.11
Only_EMISS_NE	-24.45	-8.42	-16.04

244 The quantitative changes in regional average rainfall amounts over NE India due to the different aerosol effects
 245 induced by the aerosols in different scenarios are provided in Table 23. Region-wise values can be read from
 246 Table S45. Rainfall from region 4 was not considered due to large errors being associated with it (Fig. S410). In
 247 the baseline scenario (NOR-I), the total aerosol effect caused rainfall suppression in all three regions, with a
 248 regional total of -275.13 mm, shown in Table 23. Reductions in rainfall due to the total aerosol effect was
 249 contributed by suppressions due to both direct + semi-direct and indirect effect and was observed in all the
 250 considered regions. The highest suppression was observed in region 3 (-102.60 mm), followed by region 1 (-
 251 100.60 mm). The role of direct + semi-direct effect was observed to be minimal with a total regional suppression
 252 of -17.04 mm while the indirect effect (-258.09 mm) was responsible for almost the whole of the suppression of
 253 -275.13 mm. Region 1 observed the highest suppression of -13.21 mm due to direct + semi-direct effect as this
 254 region's radiation was highest impacted by these effects.

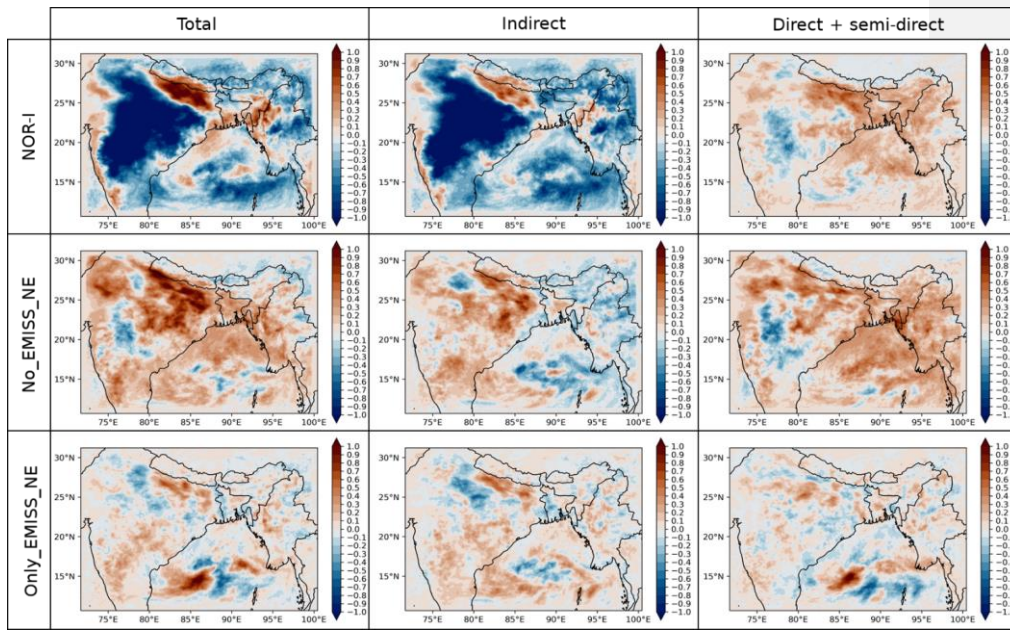
255 Direct effect could suppress rainfall by reducing surface evaporation and convection through surface
 256 dimming while semi-direct by evaporation of clouds (Talukdar et al., 2019; Lohmann and Feichter, 2001; Habib
 257 et al., 2006; Bollasina et al., 2011; Koch and Del Genio, 2010b). However, the surface dimming by indirect effect
 258 (-23.92 W m⁻²) with NOR-I was much larger than the combined direct + semi-direct effect (-3.96 W m⁻²). Hence
 259 the reduction in surface moisture flux due to indirect effect (-6.45×10⁻⁶ kg m⁻² s⁻¹) was much greater than due to
 260 combined direct + semi-direct effect (-1.1×10⁻⁶ kg m⁻² s⁻¹) and much similar to the reduction due to total aerosol
 261 effect (-7.56×10⁻⁶ kg m⁻² s⁻¹). This was also observed in the case of No_EMISS_NE. The greater surface dimming
 262 of -17.02 W m⁻² in No_EMISS_NE caused a much higher negative surface moisture flux change of -3.82×10⁻⁶ kg
 263 m⁻² s⁻¹ due to total aerosol effect, mostly contributed by indirect effect (-2.79×10⁻⁶ kg m⁻² s⁻¹) compared to direct
 264 + semi-direct effect (-1.03×10⁻⁶ kg m⁻² s⁻¹). Hence, indirect effect in NOR-I and No_EMISS_NE dominated
 265 moisture reduction through reduction in surface moisture flux over most areas of NE India at both low and high-
 266 terrain regions, as seen in Fig. 34.

Formatted: Normal, Don't keep with next

Formatted: Suppress line numbers, Position:
 Horizontal: Left, Relative to: Column, Vertical: In line,
 Relative to: Margin, Horizontal: 0 cm, Wrap Around

Formatted Table

267 However, direct + semi-direct effect caused an increase of moisture in NOR-I and No_EMISS_NE over
 268 most of NE India in spite of a negative surface moisture flux not observed in Only_EMISS_NE. This indicated
 269 that direct + semi-direct caused an increase in the transport of moisture from another region, in this case from Bay
 270 of Bengal. The equivalent potential temperature (EPT) profiles in Fig. 45 compared the atmospheric stability due
 271 to

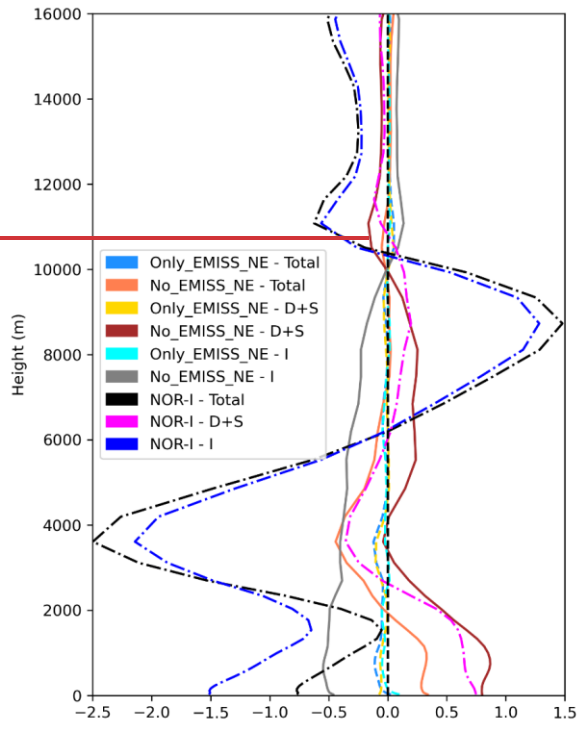


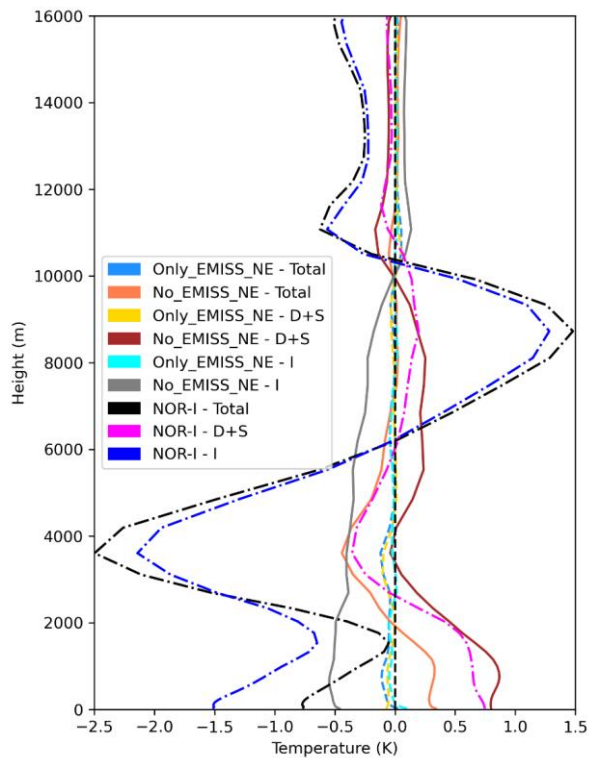
272
 273 Figure 34: Spatial distribution of change in near-surface water vapor mixing ratio (g kg^{-1}) due to total aerosol
 274 effect, direct + semi-direct effect and indirect effect

275 different aerosol effects. The greater surface dimming due to the indirect effect in No_EMISS_NE caused not
 276 only negative surface moisture flux but also a significant increase in atmospheric stability (indicated by increasing
 277 value of indirect effect EPT profile with height), reducing convection, which possibly also contributed reduction
 278 to rainfall suppression. However, although the direct + semi-direct EPT profile showed increased atmospheric
 279 stability below 1 km, but created an overall unstable atmosphere in the lower atmosphere. This instability,
 280 primarily caused due to atmospheric heating of BC, created an unstable region over NE India which facilitated
 281 the increased transport of moisture from the Bay of Bengal (discussed later). Hence, though the direct effect
 282 reduces rainfall by reducing surface moisture flux and convection but also possibly enhances it by transporting
 283 moisture. This transported moisture possibly compensated to some extent the rainfall reduction due to a decrease
 284 in surface moisture flux, convection and cloud evaporation caused by direct and semi-direct effects. Hence, the
 285 rainfall reduction due to direct + semi-direct effect (-17.04 mm) was possibly significantly less than the indirect
 286 effect (-258.09 mm). Thus, the effect of direct and indirect effects on dynamics was distinctly different. The EPT
 287 profile of the total aerosol effect in No_EMISS_NE showed an unstable lower atmosphere, supporting moisture
 288 transport. Similar explanation could be given for moisture increase due to direct + semi-direct in NOR-I but the

289 increase in atmospheric stability and moisture reduction due to greater surface dimming by its indirect effect was
290 significantly larger, which created an overall stable atmosphere due to total aerosol effect in NOR-I. The EPT
291 profiles of Only_EMITSS_NE showed almost zero perturbation throughout the atmosphere and hence was unable
292 to affect atmospheric stability and cause moisture transport. Thus, the direct + semi-direct effect in
293 Only_EMITSS_NE did not show significant moisture change in Fig. 34. Moreover, the significantly smaller surface
294 dimming (-1.21 W m^{-2}) in Only_EMITSS_NE caused very small but positive change of $8.15 \times 10^{-8} \text{ kg m}^{-2} \text{ s}^{-1}$ due to
295 the total aerosol effect and hence similar moisture change is observed in Fig. 34. Hence aerosols emitted solely
296 from NE India had negligible capability in affecting moisture through different aerosol effects. Moisture reduction
297 over NE India was much greater due to the indirect effect in No_EMITSS_NE compared to Only_EMITSS_NE,
298 while moisture increase was much greater in No_EMITSS_NE compared to Only_EMITSS_NE due to a higher
299 direct + semi-direct effect.

300

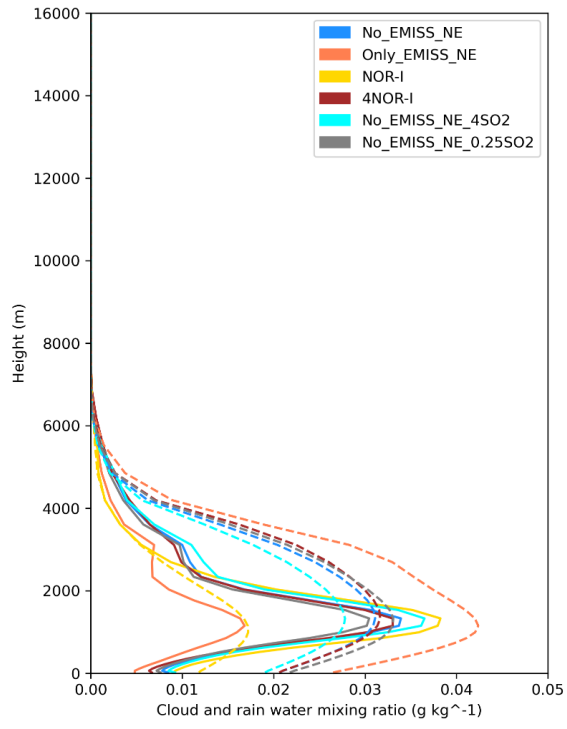




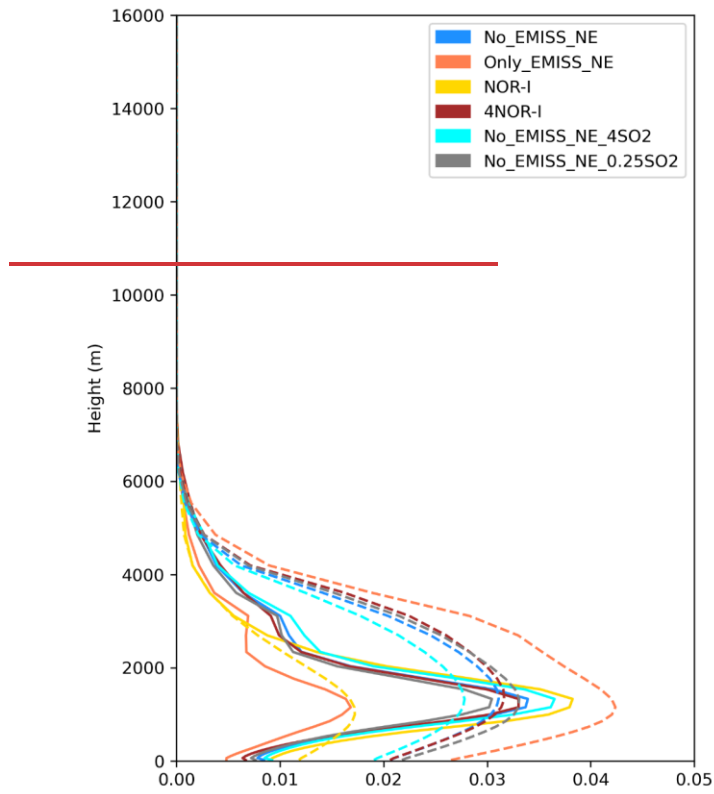
301

302 Figure 45: Perturbation of EPT (K) due to total aerosol effect (Total), direct + semi-direct (D+S) and indirect (I) aerosol effect
 303 in No_EMISS_NE (non-dashed), Only_EMISS_NE (dashed) and NOR-I (dashdot)

304 Moreover, the positive NE India regional average difference of column integrated cloud condensation
 305 nuclei (CCN) number ($4.38 \times 10^{10} \text{ m}^{-2}$), cloud droplet number ($4.42 \times 10^{13} \text{ m}^{-2}$) and cloudwater (27.93 g m^{-2}), and
 306 estimated from No_EMISS_NE – Only_EMISS_NE indicated that transported aerosols had a greater impact
 307 through aerosol indirect effect (Zhang et al., 2010). The presence of larger aerosol amounts in the form of CCN
 308 affects the cloud lifetime by affecting the conversion from cloudwater to rainwater, thus, to rainfall, thereby
 309 suppressing rainfall, also known as the 2nd indirect effect (Shiogama et al., 2010; Cherian et al., 2017). The
 310 presence of a large amount of CCN facilitates condensation of water vapor on numerous CCN particles, producing
 311 numerous cloud droplets with smaller radii. This restricts small cloud droplets to grow in size due to reduction in
 312 interaction with other cloud droplets which affect its conversion to rain droplet, and thus to rainfall. Due to more
 313 aerosol mass over NE India (Sect. 3.1), NOR-I and No_EMISS_NE had significantly higher cloudwater compared
 314 to



Formatted: Centered



316

317 Figure 56: NE India regional average vertical profiles of cloudwater mixing ratio (non-dashed) and rainwater mixing ratio
 318 (dashed) in different scenarios (g kg^{-1})

319 Only_EMISS_NE, as seen in Fig. 56. Consequently, NOR-I and No_EMISS_NE had a significantly lower
 320 rainwater mixing ratio than Only_EMISS_NE. Thus, rainfall suppression due to indirect effect was highest in
 321 NOR-I, followed by No_EMISS_NE and Only_EMISS_NE. Hence, the combined effect of reduction in moisture,
 322 instability and rainfall formation contributed to the reduction in rainfall through indirect and total aerosol effects.
 323 This could be a possible key mechanism associated with the decreasing rainfall trend in the region. Reduction of
 324 moisture due to the direct effect of aerosols and evaporation of clouds by BC were found to be possible
 325 mechanisms by Barman and Gokhale (2022). However, this study shows that the contribution of direct and semi-
 326 direct effects was very small compared to the indirect effect. The indirect effect has been found to be the dominant
 327 aerosol effect in many studies (Wang et al., 2015; Liu et al., 2016) and was found to suppress monsoon rainfall
 328 over India (Manoj et al., 2012). Aerosol indirect effect is mainly dictated by the warm clouds (Christensen et al.,
 329 2016). Thus, the higher cloud cover associated with NOR-I and No_EMISS_NE in lower atmosphere which
 330 affected SW radiation more in Sect. 3.2, was due to a greater amount of cloudwater in lower atmosphere.

331 Moreover, No_EMISS_NE and Only_EMISS_NE simulations were evaluated against the IMD rainfall
 332 dataset and NOR-I simulation to check whether the local or transported aerosols had greater control over the

333 rainfall in NE India. No_EMISS_NE showed better regional average rainfall statistics than Only_EMISS_NE
 334 with higher IOA (0.48 vs. 0.47), lower RMSE (18.85 vs. 20.37 mm day⁻¹), and lower ME (6.94 vs. 8.22 mm day⁻¹)
 335 ¹) on comparing with the IMD rainfall dataset. Also, the simulated rainfall of No_EMISS_NE showed higher
 336 rainfall similarity with NOR-I than Only_EMISS_NE with higher IOA (0.65 vs. 0.63), lower RMSE (56.32 vs.
 337 61.92 mm day⁻¹) and lower ME (39.30 vs. 39.81 mm day⁻¹). Hence, No_EMISS_NE showed more similarity with
 338 the baseline scenario as well as observed data and had greater control over the region's rainfall.

339 3.4 Role of local and transported BC

340 In section 3.3, the direct effect showed to increase moisture over NE India through an increase in atmospheric
 341 instability, caused mainly due to atmospheric heating of BC (Barman and Gokhale (2022)) Hence, to negate the
 342 effects of the indirect effect on atmospheric dynamics, scenarios in Table 1 containing only direct and semi-direct
 343 effects were used in this analysis. Moreover, NOR gave a much better performance with BC concentration
 344 estimation (Table S2) than when the indirect effect was included (NOR-I). The results from No_EMISS_NE,
 345 Only_EMISS_NE, No_NE_BCI and Only_NE_BCI scenarios were compared and related.

346 3.4.1 Radiative heating

347 The regional average vertical profiles of NOR, 2NOR, No_NE_BC, No_NE_2×BC, Only_NE_BC and
 348 Only_NE_2×BC can be seen from Fig. S511, in which the transported BC and local BC profiles resemble the
 349 No_EMISS_NE and Only_EMISS_NE PM₁₀ profiles, respectively. IGP was the dominant source of transported
 350 BC (Fig. S612). In transported BC scenarios, BC was available up to much higher atmospheric height and profiles
 351 showed elevated concentration at around 1500 m indicating stronger BC transport at that height. In Only_NE_BC
 352 and Only_NE_2×BC, BC was confined near the surface, which decreased continuously. The atmospheric heating
 353 rate (HR) was estimated as per Liou (1980).

$$354 \text{ HR} = \frac{g}{C_p} \cdot \frac{\Delta F}{\Delta P}, \quad (4)$$

355 where g is the acceleration due to gravity (9.81 m s⁻²), C_p is the specific heat capacity of air at constant pressure
 356 (1.005 kJ K⁻¹ kg⁻¹), ΔF the atmospheric RF and ΔP is the atmospheric pressure (300 hPa) difference between
 357 surface and 3 km altitude as most of the BC was present below this height. Moreover, in order to compare the
 358 effectiveness of heating by local and transported BC, two parameters, heating efficiency (HE) and heating slope
 359 (HS), were defined by equations 5 and 6.

$$360 \text{ HE} = \frac{\text{HR}}{\text{Column sum of BC concentration within 3 km (CC)}}, \quad (5)$$

$$361 \text{ HS} = \frac{\Delta \text{HR}}{\Delta \text{CC}}, \quad (6)$$

362 HE has units of K day⁻¹ μg⁻¹ m³, thus measuring the heating contributed by per unit concentration of BC below 3
 363 km. HE was used to assess the effect of BC vertical distribution on atmospheric heating while HS was used to
 364 assess the response of atmospheric heating rate to BC concentration changes and has similar units as HE. CC has
 365 units of μg m⁻³.

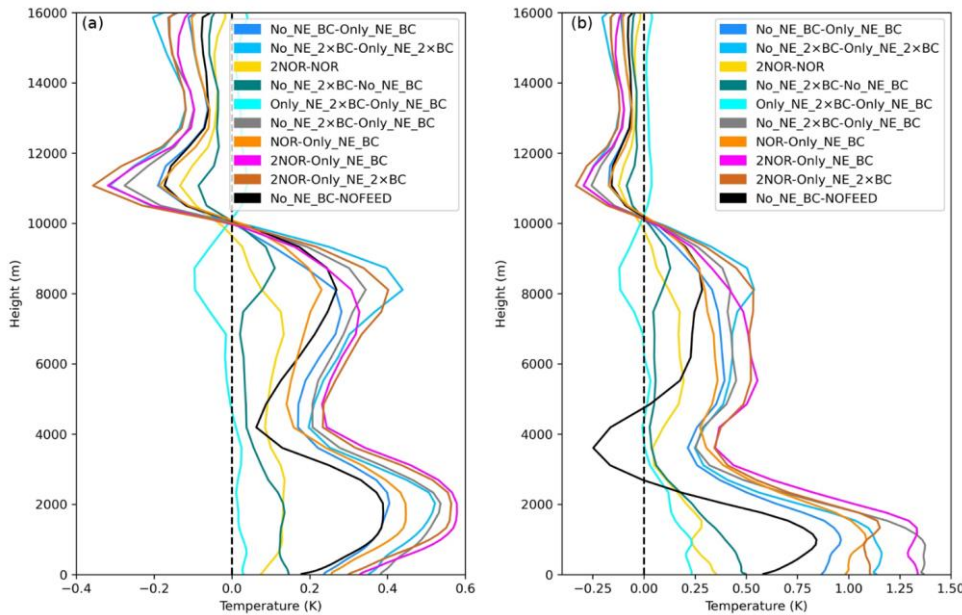
366 Table 43: NE India region average values of columnar BC concentration ($\mu\text{g m}^{-3}$) and atmospheric heating
 367 parameters in different scenarios

	No_NE_BC	No_NE_2×BC	Only_NE_BC	Only_NE_2×BC
HR	0.460	0.597	0.123	0.178
CC	12.458	18.391	3.905	7.563
HE	0.037	0.032	0.032	0.024
ΔHE	-0.004		-0.008	
HS	0.023		0.015	

Formatted Table

368 The quantitative values of the parameters are provided in Table 43. Only_NE_BC had a regional net average HR
 369 of 0.123 K day^{-1} compared to 0.460 K day^{-1} of No_NE_BC. This indicated a 3.73 times higher atmospheric heating
 370 rate by transported BC. An increase in local emissions from Only_NE_BC to Only_NE_2×BC caused a small
 371 increase in heating rate of 0.055 K day^{-1} compared to the increase of 0.137 K day^{-1} from No_NE_BC to
 372 No_NE_2×BC. As per the definition, HE was inversely proportional to CC and this was exactly followed in all
 373 regions across all scenarios (Fig. S713 and S814). However, HE was higher in the case of transported BC
 374 compared to local BC with values of $0.037 \text{ K day}^{-1} \mu\text{g}^{-1} \text{ m}^3$ (No_NE_BC) vs. $0.032 \text{ K day}^{-1} \mu\text{g}^{-1} \text{ m}^3$ (Only_NE_BC)
 375 and $0.032 \text{ K day}^{-1} \mu\text{g}^{-1} \text{ m}^3$ (No_NE_2×BC) vs. $0.024 \text{ K day}^{-1} \mu\text{g}^{-1} \text{ m}^3$ (Only_NE_2×BC), even if CC was higher
 376 in the case of transported BC. The reason might be that transported BC might have undergone a higher amount of
 377 chemical transformation due to higher atmospheric time, leading to a higher lensing effect on the BC core,
 378 resulting in enhanced absorption (Liu et al., 2015). Also, it was observed that on increasing emissions, the decrease
 379 in HE was smaller in the case of transported BC ($-0.004 \text{ K day}^{-1} \mu\text{g}^{-1} \text{ m}^3$) than local BC ($-0.008 \text{ K day}^{-1} \mu\text{g}^{-1} \text{ m}^3$).
 380 Hence, with the increase in BC emissions, HE decreased more when BC was more concentrated near the surface
 381 than in the atmosphere. HS indicated that atmospheric heating increased at a higher rate of $0.023 \text{ K day}^{-1} \mu\text{g}^{-1} \text{ m}^3$
 382 with increasing transported BC compared to $0.015 \text{ K day}^{-1} \mu\text{g}^{-1} \text{ m}^3$. Thus, the increase in transported BC emissions
 383 had more impact on atmospheric heating over NE India than when present near the surface with local emissions.

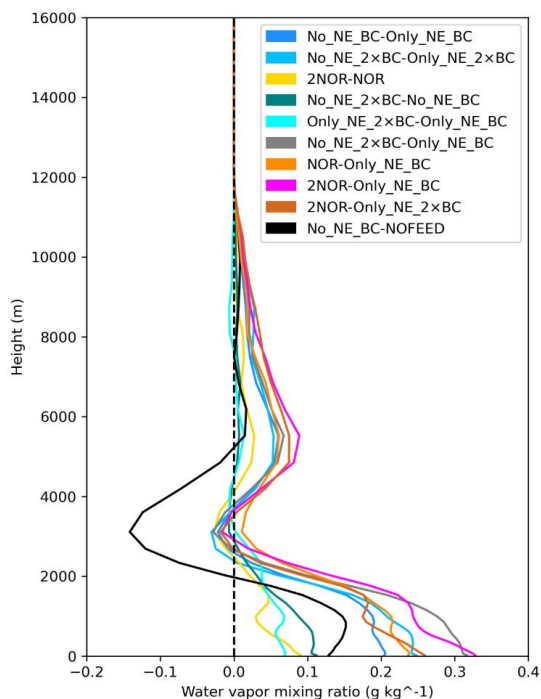
384 3.4.2 Atmospheric stability and moisture



385

386 Figure 67: Regionally averaged vertical profiles showing perturbations in a) potential temperature (K) b)
 387 equivalent potential temperature (K)

388 Barman and Gokhale (2022), as well as Soni et al. (2017), showed an increased influx of moisture into the region
 389 during pre-monsoon due to BC. In order to compare and separate the effects of local and transported BC on
 390 atmospheric stability through temperature and moisture, potential temperature (PT) and EPT were estimated. PT
 391 estimates atmospheric stability based on temperature, while EPT accounts for both temperature and moisture and
 392 is a more realistic parameter. In most of the profiles in both parameters in Fig. 76(a) and 76(b), positive
 393 perturbation was observed approximately below 10 km and negative above it which indicated an increase in
 394 atmospheric instability and vice-versa for an increase in atmospheric stability—(Zhao et al., 2011). The positive
 395 perturbations below 10 km varied with height and were most profound in the profiles No_NE_BC –
 396 Only_NE_BC, No_NE_2xBC – Only_NE_2xBC and No_NE_2xBC – Only_NE_BC, each of which was
 397 estimated from the difference between a transported BC scenario and local BC scenario. These profiles showed
 398 similarity with the corresponding profiles of NOR – Only_NE_BC, 2NOR – Only_NE_2xBC and 2NOR –
 399 Only_NE_BC in both the parameters, indicating that they were closer to the normal atmospheric scenario. The
 400 positive perturbations were, however, comparatively smaller with 2NOR – NOR, No_NE_2xBC – No_NE_BC
 401 and Only_NE_2xBC – Only_NE_BC in both the parameters, each pair being the same scenario with only a
 402 difference in emission rates. This shows that BC atmospheric distribution played an important role on instability.
 403 The Only_NE_2xBC – Only_NE_BC profile not only showed a smaller increase in instability than No_NE_2xBC
 404 – No_NE_BC profile but also contributed to the smallest increase in instability in both the parameters. Thus,
 405 transported BC and an increase in transported BC emissions led to higher atmospheric instability than local BC.



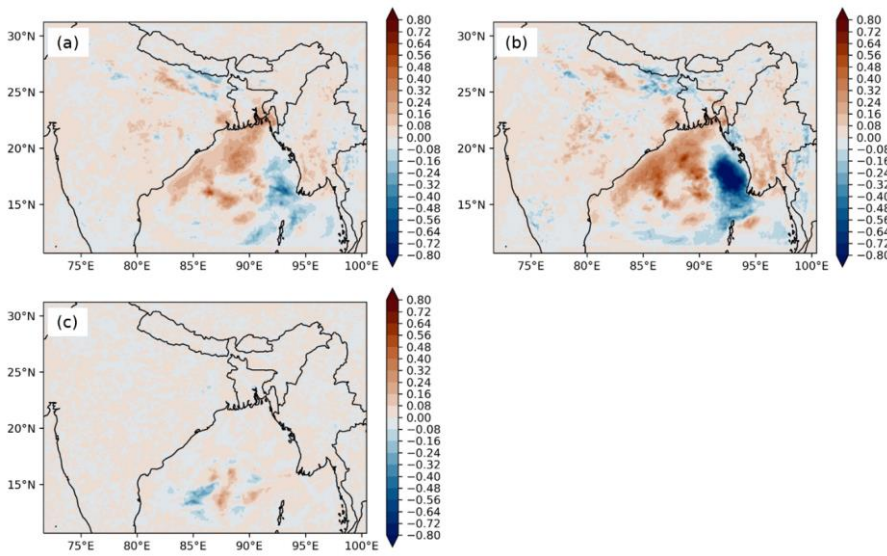
406

407 Figure 78: Regionally averaged vertical profiles showing perturbations in water vapor mixing ratio (g kg^{-1})

408 Moreover, EPT profiles showed higher positive perturbations and hence higher instability compared to
 409 the corresponding PT profiles with values exceeding 1.25 K. The positive difference or additional instability
 410 between the corresponding profiles of Fig. 76(a) and 76(b) was due to moisture. The difference also indicated that
 411 moisture contributed even more to the instability than BC. The peaks for EPT existed closer to the surface due to
 412 most of the moisture also remaining near the surface, as shown in Fig. 87. However, there occurred a region of
 413 increased stability from the ground surface to the first peak of transported BC profiles at approximately 1000 m,
 414 indicated by increasing temperature with height. Thus, transported BC may also be responsible for air quality
 415 scenarios over NE India by creating a stable boundary layer. The close qualitative and quantitative similarity
 416 between No_NE_BC – NOFEED, No_NE_BC – Only_NE_BC and NOR – Only_NE_BC profiles in Fig. 76(a)
 417 showed that aerosol radiative effect due to transported BC was intricately linked with the PT profile and the
 418 positive perturbations in each of these profiles were also closely linked with BC. This was also seen in Fig. 76(b),
 419 but since it also included the effect of moisture, larger differences were seen.

420 BC, whether transported or emitted locally, caused a positive perturbation in moisture at least below 2
 421 km altitude, as seen in Fig. 87. The perturbation was much larger in profiles that had a combination of transported
 422 and local BC scenarios and which had higher transported BC emissions and followed the pattern similar to PT
 423 and EPT. This links BC, instability and moisture in the region, i.e., higher transported BC caused higher instability
 424 which brought a higher amount of moisture which would possibly again cause higher instability. It was the same

425 for scenarios that included indirect effect, as can be observed from the similarities of the No_NE_BCI –
 426 Only_NE_BCI (Fig. S915) and No_NE_BC – Only_NE_BC profile in Fig.78. Furthermore, the similarity of
 427 No_EMISS_NE – Only_EMISS_NE profile with No_NE_BCI – Only_NE_BCI (Fig. S159) inferred that direct
 428 radiative effect of transported BC was responsible for the moisture increase in Fig. 34. The higher moisture with
 429 transported BC scenarios was due to higher moisture flux caused by it over Bay of Bengal compared to local BC
 430 and can be verified from Fig. S409. Quantitatively, No_NE_BC (33.95 kg m^{-2}) and No_NE_2×BC (34.15 kg m^{-2})
 431 had higher region average precipitable water vapor than Only_NE_BC (33.49 kg m^{-2}) and Only_NE_2×BC
 432 (33.64 kg m^{-2}). Hence transported BC in Sect. 3.3 was primarily responsible for transporting moisture from the
 433 Bay of Bengal by affecting the atmospheric dynamics. The mechanism is similar to the "heat pump" model by
 434 Lau et al. (2006).



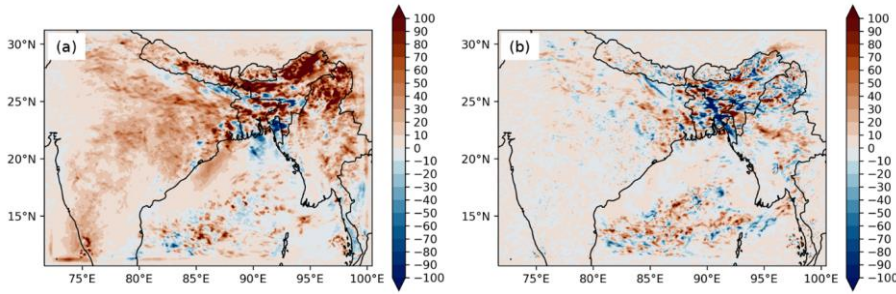
435
 436 **Figure 9: Spatial distributions of change in moisture flux ($\text{g s}^{-1} \text{ m}^{-2}$) in a) No_NE_BC – Only_NE_BC b)**
 437 **No_NE_2×BC – Only_NE_BC c) Only_NE_2×BC – Only_NE_BC near surface**

438
 439 **3.5 Rainfall response to emissions**

440 Similar to NOR-I – NOCHEM, No_BC_ABS – NOCHEM gave the rainfall change due to total aerosol effect,
 441 but without BC absorption. The higher negative rainfall change of -275.13 mm with NOR-I – NOCHEM
 442 compared to -266.78 mm with No_BC_ABS – NOCHEM showed BC absorption to reduce rainfall. The higher
 443 reduction with NOR-I – NOCHEM was mainly due to higher rainfall reduction in region 1, where the direct and
 444 semi-direct effect was maximum. This shows BC initially suppressed rainfall even though moisture increased due
 445 to it. However, with the increase in BC emissions, rainfall increased and the rainfall suppression due to the total
 446 aerosol effect reduced substantially to -64.44 mm with 4NOR-I – NOCHEM compared to -275.13 mm with NOR-

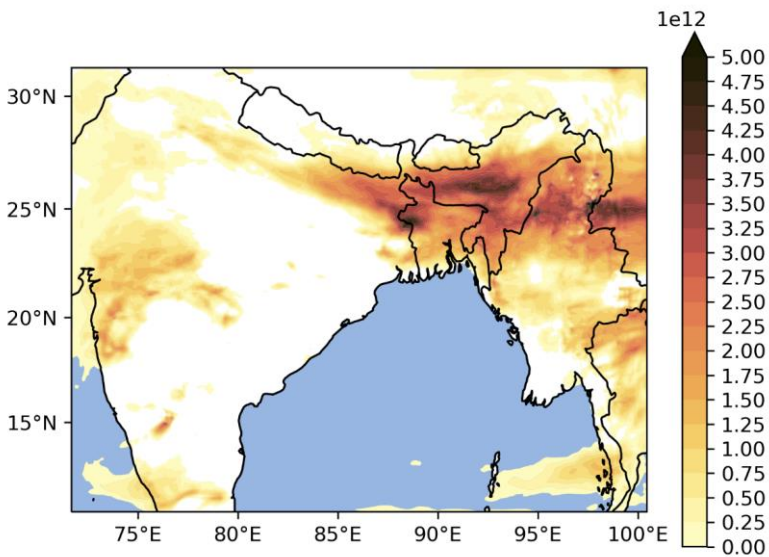
Formatted: Indent: First line: 0 cm

447 I – NOCHEM and similarly, rainfall due to direct and semi-direct with 4NOR-I – NOFEED-I showed a positive
 448 rainfall change of 193.64 mm compared to -17.04 mm with NOR-I – NOFEED. Similarly, 4NOR-I – NOR-I gave
 449 a rainfall enhancement of 225.24 mm. Spatial distribution of change in rainfall is shown in Fig. 10(a) which show
 450 rainfall change primarily occurring over NE India and along the valley.



451
 452 Figure 10: Spatial distributions of change in rainfall (mm) in a) 4NOR-I – NOR-I b) No EMISS_NE 4SO₂ =
 453 No EMISS_NE 0.25SO₂

454 Aged BC also contributes as CCN (Lambe et al., 2015). The enhancement in BC emission did increase the column
 455 average CCN concentration to 2252 m⁻³ (4NOR-I) from 2024 m⁻³ (NOR-I), but the increase was largely
 456 disproportionate to the 4 times BC emission increase. The enhancement over NE India can also be seen from the
 457 spatial distribution of column integrated CCN in Fig. 11.



458
 459 Figure 11: Spatial distribution of column integrated CCN number (m⁻²), estimated from 4NOR-I – NOR-I.

Formatted: Keep with next

Formatted: Font: 10 pt, Not Italic, Font color: Auto, Complex Script Font: 10 pt, Not Italic

Formatted: Font: 10 pt, Not Italic, Font color: Auto, Complex Script Font: 10 pt, Not Italic

Formatted: Font: 10 pt, Not Italic, Font color: Auto, Complex Script Font: 10 pt, Not Italic

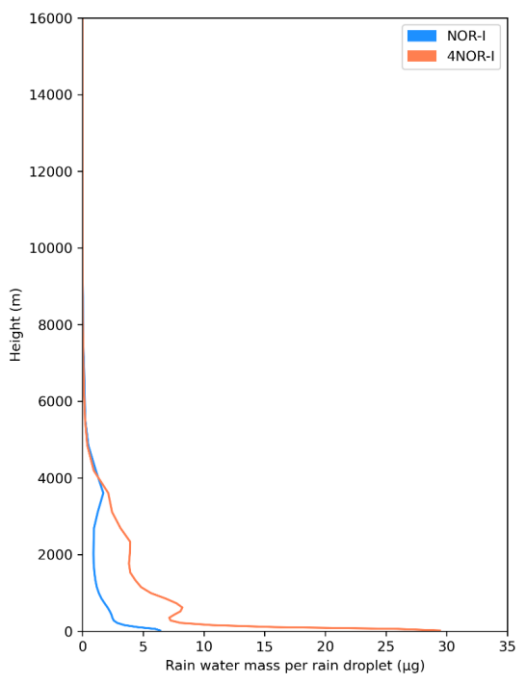
Formatted: Font: 10 pt, Not Italic, Font color: Auto, Complex Script Font: 10 pt, Not Italic

Formatted: Font: 10 pt, Not Italic, Font color: Auto, Complex Script Font: 10 pt, Not Italic

Formatted: Font: 11 pt, Complex Script Font: 11 pt

Formatted: Caption, Line spacing: single

460 Enhancement of CCN number concentration generally leads to enhancement of indirect aerosol effect (Yu et al.,
 461 2013) and also seen later in case of sulfate aerosol. However, in spite of the increase in CCN, cloudwater mixing
 462 ratio was lower in 4NOR-I than NOR-I, as seen in Fig. 56 and 4NOR-I caused significantly more rainfall
 463 formation than NOR-I, as can be seen from the rainwater mixing ratio profiles. This may be related to the
 464 suppression of CCN activation due to BC, as observed over Central India (Nair Jayachandran et al., 2020). Also
 465 BC contributes marginally to indirect effect (Kristjánsson, 2002). Thus, the increased moisture (Fig. S915) did
 466 not remain stored as cloudwater even though there was an increase in CCN, but it got converted to rainwater. The
 467 large increase in moisture, caused by the increase in atmospheric instability possibly condensed on relatively a
 468 smaller number of CCN particles promoting larger cloud droplets which enhanced rainfall. Moreover, the ratio of
 469 rainwater mixing ratio to rain droplet number concentration gave the amount of rain water per rain droplet, or
 470 indirectly the rain droplet size. The vertical profile of this ratio is shown in Figure 12, which shows higher values
 471 for 4NOR-I.



472

473 Figure 12: NE India region averaged vertical profiles of rain water mass per rain droplet.

474 Collision is the primary mechanism of rain development in warm clouds (Lamb and Verlinde, 2011). Since rain
 475 droplets are formed from the gathering of cloud droplets, the higher value for 4NOR-I indicated larger rain droplet
 476 formation, possibly through better collisions among the cloud droplets, besides higher moisture availability. This
 477 indicated that the increase in BC emissions didn't contribute to rainfall suppression through indirect aerosol effect
 478 though there was an increase in CCN concentration, but rather counteracted the suppression of rainfall due to the
 479 indirect effect of other aerosol species. The rainfall enhancement was due to an increase in moisture, contributed

Formatted: Keep with next

Formatted: Font: 10 pt, Not Italic, Font color: Auto, Complex Script Font: 10 pt, Not Italic

Formatted: Font: 10 pt, Not Italic, Font color: Auto, Complex Script Font: 10 pt, Not Italic

Formatted: Font: 11 pt, Complex Script Font: 11 pt

Formatted: Caption, Line spacing: single

480 by the transported fraction of BC, as explained in Sect. 3.4.2. Moreover, rainfall suppression was also more due
481 to transported aerosols, mainly contributed by indirect effect (Table 23).

482 Also, among the non-absorbing aerosols, sulfate aerosol is an important contributor to CCN and indirect
483 effect (Kristjánsson, 2002). Its concentration was found to be the highest among non-absorbing aerosols and most
484 of its mass over NE India was found to be transported (Sect. 3.1). Concentration profiles can be seen from Fig.
485 S146. Hence, the response of rainfall over NE India was checked by increasing (No_EMISS_NE_4SO₂) and
486 decreasing (No_EMISS_NE_0.25SO₂) SO₂ emissions outside NE India and compared against the baseline
487 transported scenario (No_EMISS_NE) since sulfate is mainly formed within the atmosphere by oxidation of SO₂
488 (Wang et al., 2021). Similar to the increase in BC emissions, No_EMISS_NE_4SO₂ caused an increase in column
489 average CCN concentration to 3524 m⁻³ compared to 1753 m⁻³ in No_EMISS_NE, while
490 No_EMISS_NE_0.25SO₂ showed a decrease (1390 m⁻³). However, contrary to the BC, an increase in SO₂
491 emissions with No_EMISS_NE_4SO₂ caused an increase in cloudwater mixing ratio compared to
492 No_EMISS_NE, as seen in Fig. 56, while its decrease also caused a decrease. Thus, No_EMISS_NE_4SO₂ and
493 No_EMISS_NE_0.25SO₂ had lower and higher rainwater mixing ratio, respectively, compared to
494 No_EMISS_NE. Consequently, No_EMISS_NE_4SO₂ had higher rainfall suppression and gave lesser rainfall (-
495 22.23 mm) compared to No_EMISS_NE_0.25SO₂. Spatial distribution is shown in Fig. 10(b) which show mainly
496 negative change over the region. Thus, an increase in non-absorbing aerosol caused rainfall suppression through
497 indirect effect. The indirect effect was observed to be the dominant aerosol effect for suppressing rainfall.
498 However, with an increase in BC, suppression of rainfall due to direct and semi-direct effects through surface
499 processes (surface moisture flux, convection) and cloud evaporation as well as due to indirect aerosol effect
500 (atmospheric stability, surface moisture flux and cloud to rainwater conversion) becomes comparatively weaker
501 mechanisms than the direct effect of radiative heating by BC, enhancing rainfall through the transport of moisture.
502 However, the increase in transported SO₂ emissions also caused further suppression of rainfall. Hence, an increase
503 in transported aerosols of an absorbing aerosol (BC) and a non-absorbing aerosol (sulfate), both being a
504 contributor to CCN, ~~showed different responses exerted different impacts~~ to indirect effect parameters and thus
505 to rainfall and hence most likely controls the enhancement and suppression of pre-monsoon rainfall over NE India,
506 thus counteracting each other. However, since decreasing rainfall trend has been observed, the impacts of the
507 indirect aerosol effect could be dominant. Here, the response of only one non-absorbing aerosol (sulfate) was
508 checked and possibly has contributions from other similar species also. ~~Other non-absorbing aerosol species like~~
509 ~~nitrate also contribute to indirect aerosol effect~~ (Wang et al., 2010; Zaveri et al., 2021) which may contribute to
510 rainfall suppression as sulfate.

511 Moreover, the percentage of the simulation time different aerosol effects and BC emissions increased
512 (inc) or suppressed (dec) rainfall under different rainfall intensities (low: 0-5, medium: 5-10, high: > 10 mm day⁻¹;
513 defined as per (Raju et al., 2015)) and the rainfall amount under those intensities was estimated. Regional
514 average values are provided in Table S56 and S67. All aerosol effects caused a higher decrease across all rainfall
515 intensities, except the indirect effect, which indicated a higher increase in low-intensity rainfall (6.52 mm vs. -
516 6.48 mm; 21.44 % vs. 20.58 %). High-intensity rain was primarily responsible for rainfall changes across all the
517 scenarios and effects. The indirect effect decreased high-intensity rainfall duration (18.85 vs. 12.38 %) and amount
518 (-399.41 mm vs. 141.62 mm) and was primarily responsible for the rainfall suppression in total aerosol effect (-

519 411.34 mm). The total aerosol effect with enhanced BC emissions (4NOR-I – NOCHEM) showed a significantly
520 higher increase (275.47 mm vs. 137.16 mm) as well as a significantly lower decrease (-337.23 vs. -411.34) in
521 high-intensity rainfall compared to total aerosol effect with baseline BC emissions (NOR-I – NOCHEM). Similar
522 results in time and rainfall amount between BC increase and direct + semi-direct effect with BC increase scenarios
523 inferred that enhanced radiative effects due to BC increase were mainly responsible for higher high-intensity
524 rainfall duration and rainfall amount, while the indirect aerosol effect was mainly involved in its suppression,
525 possibly due to the increased atmospheric stability associated with it. Barman and Gokhale (2022) also showed
526 similar results with BC emissions increase, but this study verifies the role of direct radiative effects of BC in it.
527 Thus, BC increased rainfall over NE India but in the form of high-intensity rainfall. Hence, relative fractions of
528 BC and the other aerosols contributing to indirect effect possibly decide the amount of rainfall and its intensity
529 over the region. However, indirect effect also caused high-intensity rainfall but with lesser amount than its
530 suppression and may be involved in catastrophic flood events at local scales (Wang et al., 2022).

531 **4 Conclusions**

532 Transported aerosols, primarily from IGP, were found to be responsible for the bulk of the aerosol mass (93.98
533 %) over NE India while contributing 64.18 % of near-surface PM₁₀ concentration, thus primarily responsible for
534 air pollution as climatic impacts over the region during pre-monsoon season. The climatic impacts, both w.r.t. RF
535 as well as rainfall, were dominated by the indirect aerosol effect. The impacts of the indirect aerosol effects of
536 transported aerosols were much higher in affecting radiation (-13.12 W m⁻² vs. -0.24 W m⁻² at the surface, 7.30 W
537 m⁻² vs. 0.97 W m⁻² in the atmosphere) as well as suppressing rainfall (-49.11 mm vs. -16.04 mm) compared to
538 local emissions. The greater surface dimming by transported aerosols caused a higher negative change in surface
539 moisture flux (-3.82×10⁻⁶ kg m⁻² s⁻¹ vs. 8.15×10⁻⁸ kg m⁻² s⁻¹) as well as higher aerosol mass reduced cloudwater to
540 rainwater conversion, both of which contributed to higher rainfall suppression. Transported aerosols caused
541 4.42×10¹³ m⁻² higher cloud droplets than local emissions. The atmospheric instability due to the direct + semi-
542 direct effect and indirect effect of transported aerosols were found to be contradictory and caused an increase and
543 decrease, respectively. The direct effect of transported aerosols, though also caused negative surface moisture flux
544 over NE India (-1.03×10⁻⁶ kg m⁻² s⁻¹), however, increased moisture over NE India, increasing moisture flux over
545 the Bay of Bengal. Further analysis showed that transported BC was more efficient in atmospheric heating over
546 NE India and together with the higher transported BC mass, an increase in its emissions caused higher atmospheric
547 instability over the region, which brought more moisture from the Bay of Bengal. The increased moisture further
548 contributed to higher instability. Hence, the rainfall suppression caused through the different atmospheric
549 processes by direct, semi-direct and indirect effects was reduced and nullified with the increase in BC emissions,
550 but the rainfall increase was mainly in the form of high-intensity rainfall. The increase in BC did not show a
551 positive change in cloudwater, though it contributed to CCN. The direct effect of BC thus overpowered the other
552 rainfall-suppressing processes. Indirect aerosol effect and radiative heating were the main rainfall-controlling
553 factors. Hence, changes in emissions of aerosols or chemical species contributing to these processes will possibly
554 contribute to rainfall suppression and enhancement over NE India. Moreover, rainfall simulated with transported
555 aerosols were found to be more similar to the IMD observation datasets as well as the baseline emission scenario,
556 indicating its possible greater influence in the real-world scenario.

557 The study shows that the atmospheric transport of emissions from IGP to NE India has a significant
558 impact on NE India's [rainfallatmosphere](#) during pre-monsoon and the impacts are even greater than the emissions
559 within the NE India region.

560 **Data availability.** Model outputs are available upon request.

561 **Author contributions.** NB - conceptualization, methodology, model simulation, visualisation, manuscript
562 writing, SG - conceptualization, methodology and supervision, manuscript review and editing.

563 **Competing interests.** The authors declare that they have no conflict of interest.

564 **Disclaimer.** The views expressed in this paper are those of the authors.

565 **Acknowledgements.** The simulations were performed on the "Param-Ishan" HPC of Indian Institute of
566 Technology Guwahati. The authors are also grateful to "Air and Noise Pollution Lab" of Civil Department IIT
567 Guwahati for their support.

568 References

- 569 Bagtasa, G., Cayetano, M. G., Yuan, C. S., Uchino, O., Sakai, T., Izumi, T., Morino, I., Nagai, T., Macatangay,
570 R. C., and Velasco, V. A.: Long-range transport of aerosols from East and Southeast Asia to northern
571 Philippines and its direct radiative forcing effect, *Atmos. Environ.*, 218, 117007,
572 <https://doi.org/10.1016/j.atmosenv.2019.117007>, 2019.
- 573 Barman, N. and Gokhale, S.: Urban black carbon - source apportionment, emissions and long-range transport
574 over the Brahmaputra River Valley, *Sci. Total Environ.*, 693, 1–14,
575 <https://doi.org/10.1016/j.scitotenv.2019.07.383>, 2019.
- 576 Barman, N. and Gokhale, S.: Aerosol influence on the pre-monsoon rainfall mechanisms over North-East India:
577 A WRF-Chem study, *Atmos. Res.*, 268, 106002, <https://doi.org/10.1016/j.atmosres.2021.106002>, 2022.
- 578 Bauer, S. E. and Menon, S.: Aerosol direct, indirect, semidirect, and surface albedo effects from sector
579 contributions based on the IPCC AR5 emissions for preindustrial and present-day conditions,
580 <https://doi.org/10.1029/2011JD016816>, 2012.
- 581 Bhat, M. A., Romshoo, S. A., and Beig, G.: Characteristics, source apportionment and long-range transport of
582 black carbon at a high-altitude urban centre in the Kashmir valley, North-western Himalaya, *Environ. Pollut.*,
583 305, 119295, <https://doi.org/10.1016/j.envpol.2022.119295>, 2022.
- 584 Bollasina, M. A., Ming, Y., and Ramaswamy, V.: Anthropogenic aerosols and the weakening of the south asian
585 summer monsoon, *Science (80-.)*, 334, 502–505, <https://doi.org/10.1126/science.1204994>, 2011.
- 586 Bonasoni, P., Laj, P., Marinoni, A., Sprenger, M., Angelini, F., Arduini, J., Bonafè, U., Calzolari, F., Colombo,
587 T., Decesari, S., Di Biagio, C., Di Sarra, A. G., Evangelisti, F., Duchi, R., Facchini, M. C., Fuzzi, S., Gobbi, G.
588 P., Maione, M., Panday, A., Roccatò, F., Sellegri, K., Venzac, H., Verza, G. P., Villani, P., Vuillermoz, E., and
589 Cristofanelli, P.: Atmospheric Brown Clouds in the Himalayas: First two years of continuous observations at the
590 Nepal Climate Observatory-Pyramid (5079 m), *Atmos. Chem. Phys.*, 10, 7515–7531,
591 <https://doi.org/10.5194/acp-10-7515-2010>, 2010.
- 592 Bond, T. C., Doherty, S. J., Fahey, D. W., Forster, P. M., Berntsen, T., Deangelo, B. J., Flanner, M. G., Ghan,
593 S., Kärcher, B., Koch, D., Kinne, S., Kondo, Y., Quinn, P. K., Sarofim, M. C., Schultz, M. G., Schulz, M.,
594 Venkataraman, C., Zhang, H., Zhang, S., Bellouin, N., Guttikunda, S. K., Hopke, P. K., Jacobson, M. Z., Kaiser,
595 J. W., Klimont, Z., Lohmann, U., Schwarz, J. P., Shindell, D., Storelvmo, T., Warren, S. G., and Zender, C. S.:
596 Bounding the role of black carbon in the climate system: A scientific assessment, *J. Geophys. Res. Atmos.*, 118,
597 5380–5552, <https://doi.org/10.1002/jgrd.50171>, 2013.
- 598 Chatterjee, A., Adak, A., Singh, A. K., Srivastava, M. K., Ghosh, S. K., Tiwari, S., Devara, P. C. S., and Raha,
599 S.: Aerosol chemistry over a high altitude station at northeastern Himalayas, India, *PLoS One*, 5,
600 <https://doi.org/10.1371/journal.pone.0011122>, 2010.
- 601 Chaudhury, A. S., Nikhil, V. A., and Gokhale, S.: Black carbon in different climatic seasons of the Brahmaputra
602 River Valley of Northeast India – Field measurements at two different heights and analysis, *Atmos. Pollut. Res.*,
603 13, 101327, <https://doi.org/10.1016/j.apr.2022.101327>, 2022.

604 Cherian, R., Quaas, J., Salzmann, M., and Tomassini, L.: Black carbon indirect radiative effects in a climate
605 model, *Tellus, Ser. B Chem. Phys. Meteorol.*, 69, 1–10, <https://doi.org/10.1080/16000889.2017.1369342>, 2017.

606 Christensen, M. W., Chen, Y. C., and Stephens, G. L.: Aerosol indirect effect dictated by liquid clouds, *J.*
607 *Geophys. Res.*, 121, 14636–14650, <https://doi.org/10.1002/2016JD025245>, 2016.

608 Dahutia, P., Pathak, B., and Bhuyan, P. K.: Aerosols characteristics, trends and their climatic implications over
609 northeast india and adjoining South Asia, *Int. J. Climatol.*, 38, 1234–1256, <https://doi.org/10.1002/joc.5240>,
610 2018.

611 Dahutia, P., Pathak, B., and Bhuyan, P. K.: Vertical distribution of aerosols and clouds over north-eastern South
612 Asia: Aerosol-cloud interactions, *Atmos. Environ.*, 215, 116882,
613 <https://doi.org/10.1016/j.atmosenv.2019.116882>, 2019.

614 Emery, C., Tai, E., and Yarwood, G.: Enhanced Meteorological Modeling and Performance Evaluation for Two
615 Texas Ozone Episodes, *Env. Int. Corp.*, 235, 2001.

616 Emmons, L. K., Walters, S., Hess, P. G., Lamarque, J. F., Pfister, G. G., Fillmore, D., Granier, C., Guenther, A.,
617 Kinnison, D., Laepple, T., Orlando, J., Tie, X., Tyndall, G., Wiedinmyer, C., Baughcum, S. L., and Kloster, S.:
618 Description and evaluation of the Model for Ozone and Related chemical Tracers, version 4 (MOZART-4),
619 *Geosci. Model Dev.*, 3, 43–67, <https://doi.org/10.5194/gmd-3-43-2010>, 2010.

620 Ghan, S. J., Liu, X., Easter, R. C., Zaveri, R., Rasch, P. J., Yoon, J. H., and Eaton, B.: Toward a minimal
621 representation of aerosols in climate models: Comparative decomposition of aerosol direct, semidirect, and
622 indirect radiative forcing, *J. Clim.*, 25, 6461–6476, <https://doi.org/10.1175/JCLI-D-11-00650.1>, 2012.

623 Gogoi, M. M., Babu, S. S., Moorthy, K. K., Bhuyan, P. K., Pathak, B., Subba, T., Chutia, L., Kundu, S. S.,
624 Bharali, C., Borgohain, A., Guha, A., Kumar De, B., Singh, B., and Chin, M.: Radiative effects of absorbing
625 aerosols over northeastern India: Observations and model simulations, *J. Geophys. Res.*, 122, 1132–1157,
626 <https://doi.org/10.1002/2016JD025592>, 2017.

627 Granier, C., Darras, S., Denier van der Gon, H., Doubalova, J., Elguindi, N., Galle, B., Gauss, M., Guevara, M.,
628 Jalakanen, J.-P., Kuenen, J., Liousse, C., Quack, B., Simpson, D., and Sinderlova, K.: The Copernicus
629 Atmosphere Monitoring Service global and regional emissions (April 2019 version),
630 <https://doi.org/10.24380/d0bn-kx16>, 2019.

631 Grell, G. A. and Freitas, S. R.: A scale and aerosol aware stochastic convective parameterization for weather and
632 air quality modeling, *Atmos. Chem. Phys.*, 14, 5233–5250, <https://doi.org/10.5194/acp-14-5233-2014>, 2014.

633 Grell, G. A., Peckham, S. E., Schmitz, R., McKeen, S. A., Frost, G., Skamarock, W. C., and Eder, B.: Fully
634 coupled “online” chemistry within the WRF model, *Atmos. Environ.*, 39, 6957–6975,
635 <https://doi.org/10.1016/j.atmosenv.2005.04.027>, 2005.

636 Guenther, A., Karl, T., Harley, P., Wiedinmyer, C., Palmer, P. I., and Geron, C.: and Physics Estimates of global
637 terrestrial isoprene emissions using MEGAN (Model of Emissions of Gases and Aerosols from Nature), 3181–
638 3210, 2006.

639 Guha, A., De, B. K., Dhar, P., Banik, T., Chakraborty, M., Roy, R., Choudhury, A., Gogoi, M. M., Babu, S. S.,
640 and Moorthy, K. K.: Seasonal Characteristics of Aerosol Black Carbon in Relation to Long Range Transport
641 over Tripura in Northeast India, 786–798, <https://doi.org/10.4209/aaqr.2014.02.0029>, 2015.

642 Habib, G., Venkataraman, C., Chiapello, I., Ramachandran, S., Boucher, O., and Shekar Reddy, M.: Seasonal
643 and interannual variability in absorbing aerosols over India derived from TOMS: Relationship to regional
644 meteorology and emissions, *Atmos. Environ.*, 40, 1909–1921, <https://doi.org/10.1016/j.atmosenv.2005.07.077>,
645 2006.

646 Hersbach, H., Bell, B., Berrisford, P., Hirahara, S., Horányi, A., Muñoz-Sabater, J., Nicolas, J., Peubey, C.,
647 Radu, R., Schepers, D., Simmons, A., Soci, C., Abdalla, S., Abellan, X., Balsamo, G., Bechtold, P., Biavati, G.,
648 Bidlot, J., Bonavita, M., De Chiara, G., Dahlgren, P., Dee, D., Diamantakis, M., Dragani, R., Flemming, J.,
649 Forbes, R., Fuentes, M., Geer, A., Haimberger, L., Healy, S., Hogan, R. J., Hólm, E., Janisková, M., Keeley, S.,
650 Laloyaux, P., Lopez, P., Lupu, C., Radnoti, G., de Rosnay, P., Rozum, I., Vamborg, F., Villaume, S., and
651 Thépaut, J. N.: The ERA5 global reanalysis, *Q. J. R. Meteorol. Soc.*, 146, 1999–2049,
652 <https://doi.org/10.1002/qj.3803>, 2020.

653 Iacono, M. J., Delamere, J. S., Mlawer, E. J., Shephard, M. W., Clough, S. A., and Collins, W. D.: Radiative

654 forcing by long-lived greenhouse gases: Calculations with the AER radiative transfer models,
655 <https://doi.org/10.1029/2008JD009944>, 2008.

656 Kant, S., Panda, J., Rao, P., Sarangi, C., and Ghude, S. D.: Study of aerosol-cloud-precipitation-meteorology
657 interaction during a distinct weather event over the Indian region using WRF-Chem, *Atmos. Res.*, 247,
658 <https://doi.org/10.1016/j.atmosres.2020.105144>, 2021.

659 Kedia, S., Cherian, R., Islam, S., Das, S. K., and Kaginalkar, A.: Regional simulation of aerosol radiative effects
660 and their influence on rainfall over India using WRFChem model, *Atmos. Res.*, 182, 232–242,
661 <https://doi.org/10.1016/j.atmosres.2016.07.008>, 2016.

662 Kedia, S., Das, S. K., Islam, S., Hazra, A., and Kumar, N.: Aerosols impact on the convective and non-
663 convective rain distribution over the Indian region: Results from WRF-Chem simulation, *Atmos. Environ.*, 202,
664 64–74, <https://doi.org/10.1016/j.atmosenv.2019.01.020>, 2019.

665 Koch, D. and Del Genio, A. D.: Black carbon semi-direct effects on cloud cover: Review and synthesis, *Atmos.*
666 *Chem. Phys.*, 10, 7685–7696, <https://doi.org/10.5194/acp-10-7685-2010>, 2010a.

667 Koch, D. and Del Genio, A. D.: Black carbon semi-direct effects on cloud cover: Review and synthesis, *Atmos.*
668 *Chem. Phys.*, 10, 7685–7696, <https://doi.org/10.5194/acp-10-7685-2010>, 2010b.

669 Krishnamohan, K. S., Modak, A., and Bala, G.: Effects of local and remote black carbon aerosols on summer
670 monsoon precipitation over india, *Environ. Res. Commun.*, 3, <https://doi.org/10.1088/2515-7620/AC18D1>,
671 2021.

672 Kristjánsson, J. E.: Studies of the aerosol indirect effect from sulfate and black carbon aerosols, *J. Geophys.*
673 *Res. Atmos.*, 107, 1–19, <https://doi.org/https://doi.org/10.1029/2001JD000887>, 2002.

674 Kumar, M., Parmar, K. S., Kumar, D. B., Mhawish, A., Broday, D. M., Mall, R. K., and Banerjee, T.: Long-
675 term aerosol climatology over Indo-Gangetic Plain: Trend, prediction and potential source fields, *Atmos.*
676 *Environ.*, 180, 37–50, <https://doi.org/10.1016/j.atmosenv.2018.02.027>, 2018.

677 Kundu, S. S., Borgohain, A., Barman, N., Devi, M., and Raju, P. L. N.: Spatial Variability and Radiative Impact
678 of Aerosol along the Brahmaputra River Valley in India: Results from a Campaign, *J. Environ. Prot. (Irvine,*
679 *Calif.)*, 09, 405–430, <https://doi.org/10.4236/jep.2018.94026>, 2018.

680 Lamarque, J. F., Emmons, L. K., Hess, P. G., Kinnison, D. E., Tilmes, S., Vitt, F., Heald, C. L., Holland, E. A.,
681 Lauritzen, P. H., Neu, J., Orlando, J. J., Rasch, P. J., and Tyndall, G. K.: CAM-chem: Description and
682 evaluation of interactive atmospheric chemistry in the Community Earth System Model, *Geosci. Model Dev.*, 5,
683 369–411, <https://doi.org/10.5194/gmd-5-369-2012>, 2012.

684 Lamb, D. and Verlinde, J.: *PHYSICS AND CHEMISTRY OF CLOUDS*, Cambridge University Press, 2011.

685 Lambe, A. T., Ahern, A. T., Wright, J. P., Croasdale, D. R., Davidovits, P., and Onasch, T. B.: Oxidative aging
686 and cloud condensation nuclei activation of laboratory combustion soot, *J. Aerosol Sci.*, 79, 31–39,
687 <https://doi.org/10.1016/j.jaerosci.2014.10.001>, 2015.

688 Lau, K. M., Kim, M. K., and Kim, K. M.: Asian summer monsoon anomalies induced by aerosol direct forcing:
689 The role of the Tibetan Plateau, *Clim. Dyn.*, 26, 855–864, <https://doi.org/10.1007/s00382-006-0114-z>, 2006.

690 Lee, H. J., Jo, Y. J., Kim, S., Kim, D., Kim, J. M., Choi, D., Jo, H. Y., Bak, J., Park, S. Y., Jeon, W., and Kim,
691 C. H.: Transboundary aerosol transport process and its impact on aerosol-radiation-cloud feedbacks in
692 springtime over Northeast Asia, *Sci. Rep.*, 12, 1–10, <https://doi.org/10.1038/s41598-022-08854-1>, 2022.

693 Liou, K. N.: *An Introduction to Atmospheric Radiation*, 1980.

694 Liu, S., Aiken, A. C., Gorkowski, K., Dubey, M. K., Cappa, C. D., Williams, L. R., Herndon, S. C., Massoli, P.,
695 Fortner, E. C., Chhabra, P. S., Brooks, W. A., Onasch, T. B., Jayne, J. T., Worsnop, D. R., China, S., Sharma,
696 N., Mazzoleni, C., Xu, L., Ng, N. L., Liu, D., Allan, J. D., Lee, J. D., Fleming, Z. L., Mohr, C., Zotter, P.,
697 Szidat, S., and Prévôt, A. S. H.: Enhanced light absorption by mixed source black and brown carbon particles in
698 UK winter, *Nat. Commun.*, 6, <https://doi.org/10.1038/ncomms9435>, 2015.

699 Liu, X. Y., Zhang, Y., Zhang, Q., and He, K. Bin: Application of online-coupled WRF/Chem-MADRID in East
700 Asia: Model evaluation and climatic effects of anthropogenic aerosols, *Atmos. Environ.*, 124, 321–336,
701 <https://doi.org/10.1016/j.atmosenv.2015.03.052>, 2016.

702 Lohmann, U. and Feichter, J.: Can the direct and semi-direct aerosol effect compete with the indirect effect on a
703 global scale?, *Geophys. Res. Lett.*, 28, 159–161, <https://doi.org/10.1029/2000GL012051>, 2001.

704 Manoj, M. G., Devara, P. C. S., Joseph, S., and Sahai, A. K.: Aerosol indirect effect during the aberrant Indian
705 Summer Monsoon breaks of 2009, *Atmos. Environ.*, 60, 153–163,
706 <https://doi.org/10.1016/j.atmosenv.2012.06.007>, 2012.

707 Menon, S., Hansen, J., Nazarenko, L., and Luo, Y.: Climate effects of black carbon aerosols in China and India,
708 *Science* (80-.), 297, 2250–2253, <https://doi.org/10.1126/science.1075159>, 2002.

709 Mitchell, J. M.: The Effect of Atmospheric Aerosols on Climate with Special Reference to Temperature near the
710 Earth's Surface, [https://doi.org/10.1175/1520-0450\(1971\)010<0703:teoao>2.0.co;2](https://doi.org/10.1175/1520-0450(1971)010<0703:teoao>2.0.co;2), 1971.

711 Mondal, A., Lakshmi, V., and Hashemi, H.: Intercomparison of trend analysis of Multisatellite Monthly
712 Precipitation Products and Gauge Measurements for River Basins of India, *J. Hydrol.*, 565, 779–790,
713 <https://doi.org/10.1016/j.jhydrol.2018.08.083>, 2018.

714 Morrison, H., Thompson, G., and Tatarskii, V.: Impact of cloud microphysics on the development of trailing
715 stratiform precipitation in a simulated squall line: Comparison of one- and two-moment schemes, *Mon. Weather*
716 *Rev.*, 137, 991–1007, <https://doi.org/10.1175/2008MWR2556.1>, 2009.

717 Nair Jayachandran, V., Nair Suresh Babu, S., Vaishya, A., Gogoi, M. M., Nair, V. S., Krishnakumari Satheesh,
718 S., and Krishna Moorthy, K.: Altitude profiles of cloud condensation nuclei characteristics across the Indo-
719 Gangetic Plain prior to the onset of the Indian summer monsoon, *Atmos. Chem. Phys.*, 20, 561–576,
720 <https://doi.org/10.5194/acp-20-561-2020>, 2020.

721 Nair, V. S., Babu, S. S., Manoj, M. R., Moorthy, K. K., and Chin, M.: Direct radiative effects of aerosols over
722 South Asia from observations and modeling, *Clim. Dyn.*, 49, 1411–1428, <https://doi.org/10.1007/s00382-016-3384-0>, 2017.

724 Nakanishi, M. and Niino, H.: ITS NUMERICAL STABILITY AND APPLICATION TO A REGIONAL
725 PREDICTION OF ADVECTION FOG, 397–407, <https://doi.org/10.1007/s10546-005-9030-8>, 2006.

726 Nandan, R., Ratnam, M. V., Kiran, V. R., and Naik, D. N.: Aerosol-cloud interaction in water clouds observed
727 using ground-based, in-situ, and satellite-based observations over an Indian continental region, *Atmos. Res.*,
728 280, 106436, <https://doi.org/10.1016/j.atmosres.2022.106436>, 2022.

729 Nenes, A., Conant, W. C., and Seinfeld, J. H.: Black carbon radiative heating effects on cloud microphysics and
730 implications for the aerosol indirect effect 2. Cloud microphysics, *J. Geophys. Res. Atmos.*, 107, AAC 24-1-
731 AAC 24-11, <https://doi.org/10.1029/2002jd002101>, 2002.

732 Ojha, N., Naja, M., Singh, K. P., Sarangi, T., Kumar, R., Lal, S., Lawrence, M. G., Butler, T. M., and Chandola,
733 H. C.: Variabilities in ozone at a semi-urban site in the Indo-Gangetic Plain region: Association with the
734 meteorology and regional processes, *J. Geophys. Res. Atmos.*, 117, 1–19,
735 <https://doi.org/10.1029/2012JD017716>, 2012.

736 Ojha, N., Sharma, A., Kumar, M., Girach, I., Ansari, T. U., Sharma, S. K., Singh, N., Pozzer, A., and Gunthe, S.
737 S.: On the widespread enhancement in fine particulate matter across the Indo-Gangetic Plain towards winter,
738 *Sci. Rep.*, 10, 1–9, <https://doi.org/10.1038/s41598-020-62710-8>, 2020.

739 Pai, D. S., Sridhar, L., Rajeevan, M., Sreejith, O. P., Satbhai, N. S., and Mukhopadhyay, B.: Development of a
740 new high spatial resolution (0.25° × 0.25°) long period (1901–2010) daily gridded rainfall data set over India
741 and its comparison with existing data sets over the region, *Mausam*, 65, 1–18, 2014.

742 Pathak, B., Kalita, G., Bhuyan, K., Bhuyan, P. K., and Moorthy, K. K.: Aerosol temporal characteristics and its
743 impact on shortwave radiative forcing at a location in the northeast of India, 115, 1–14,
744 <https://doi.org/10.1029/2009JD013462>, 2010.

745 Pathak, B., Subba, T., Dahutia, P., Bhuyan, P. K., Moorthy, K. K., Gogoi, M. M., Babu, S. S., Chutia, L., Ajay,
746 P., Biswas, J., Bharali, C., Borgohain, A., Dhar, P., Guha, A., De, B. K., Banik, T., Chakraborty, M., Kundu, S.
747 S., Sudhakar, S., and Singh, S. B.: Aerosol characteristics in north-east India using ARFINET spectral optical
748 depth measurements, *Atmos. Environ.*, 125, 461–473, <https://doi.org/10.1016/j.atmosenv.2015.07.038>, 2016.

749 Raju, A., Parekh, A., Chowdary, J. S., and Gnanaseelan, C.: Assessment of the Indian summer monsoon in the
750 WRF regional climate model, *Clim. Dyn.*, 44, 3077–3100, <https://doi.org/10.1007/s00382-014-2295-1>, 2015.

751 Ramanathan, V., Chung, C., Kim, D., Bettge, T., Buja, L., Kiehl, J. T., Washington, W. M., Fu, Q., Sikka, D. R.,
752 and Wild, M.: Atmospheric brown clouds: Impacts on South Asian climate and hydrological cycle, *Proc. Natl.*
753 *Acad. Sci.*, 102, 5326–5333, <https://doi.org/10.1073/pnas.0500656102>, 2005.

754 Rana, A., Jia, S., and Sarkar, S.: Black carbon aerosol in India: A comprehensive review of current status and
755 future prospects, *Atmos. Res.*, 218, 207–230, <https://doi.org/10.1016/j.atmosres.2018.12.002>, 2019.

756 Rosenfeld, D.: Suppression of rain and snow by urban air pollution, *Science (80-.)*, 287, 1793–1796,
757 <https://doi.org/10.1126/science.287.5459.1793>, 2012.

758 Sarangi, C., Tripathi, S. N., Tripathi, S., and Barth, M. C.: Aerosol-cloud associations over gangetic basin
759 during a typical monsoon depression event using WRF-Chem simulation, *J. Geophys. Res.*, 120, 10,974–10,995,
760 <https://doi.org/10.1002/2015JD023634>, 2015.

761 Sarkar, C., Roy, A., Chatterjee, A., Ghosh, S. K., and Raha, S.: Factors controlling the long-term (2009–2015)
762 trend of PM 2.5 and black carbon aerosols at eastern Himalaya, India, *Sci. Total Environ.*, 656, 280–296,
763 <https://doi.org/10.1016/j.scitotenv.2018.11.367>, 2019.

764 Shiogama, H., Emori, S., Takahashi, K., Ogura, T. N., Nozawa, T., and Takemura, T.: Emission scenario
765 dependency of precipitation on global warming in the MIROC3.2 model, *J. Clim.*, 23, 2404–2417,
766 <https://doi.org/10.1175/2009JCLI3428.1>, 2010.

767 Singh, S. and Gokhale, S.: Source apportionment and light absorption properties of black and brown carbon
768 aerosols in the Brahmaputra River valley region, *Urban Clim.*, 39, 100963,
769 <https://doi.org/10.1016/j.uclim.2021.100963>, 2021.

770 Soni, P., Tripathi, S. N., and Srivastava, R.: Radiative effects of black carbon aerosols on Indian monsoon: a
771 study using WRF-Chem model, *Theor. Appl. Climatol.*, 132, 115–134, [https://doi.org/10.1007/s00704-017-](https://doi.org/10.1007/s00704-017-2057-1)
772 [2057-1](https://doi.org/10.1007/s00704-017-2057-1), 2017.

773 Talukdar, S., Venkat Ratnam, M., Ravikiran, V., and Chakraborty, R.: Influence of Black Carbon Aerosol on the
774 Atmospheric Instability, *J. Geophys. Res. Atmos.*, 124, 5539–5554, <https://doi.org/10.1029/2018JD029611>,
775 2019.

776 Tewari, M., Chen, F., Wang, W., Dudhia, J., LeMone, M. A., Mitchell, K., Ek, M., Gayno, G., Weigel, J., and
777 Cuenca, R. H.: IMPLEMENTATION AND VERIFICATION OF THE UNIFIED NOAH LAND SURFACE
778 MODEL IN THE WRF MODEL, 20th Conf. Weather Anal. Forecast. Conf. Numer. Weather Predict., 11–15,
779 <https://doi.org/10.1007/s11269-013-0452-7>, 2004.

780 Tiwari, S., Kumar, R., Tunved, P., Singh, S., and Panicker, A. S.: Significant cooling effect on the surface due
781 to soot particles over Brahmaputra River Valley region, India: An impact on regional climate, *Sci. Total*
782 *Environ.*, 562, 504–516, <https://doi.org/10.1016/j.scitotenv.2016.03.157>, 2016.

783 Tripathi, S. N., Dey, S., Tare, V., and Satheesh, S. K.: Aerosol black carbon radiative forcing at an industrial
784 city in northern India, *Geophys. Res. Lett.*, 32, 1–4, <https://doi.org/10.1029/2005GL022515>, 2005.

785 Twomey, S.: The influence of pollution on the shortwave albedo of clouds, *J. Atmos. Sci.*, 1149–1152117,
786 [https://doi.org/10.1175/1520-0469\(1977\)034<1149:TROPOT>2.0.CO;2](https://doi.org/10.1175/1520-0469(1977)034<1149:TROPOT>2.0.CO;2), 1977.

787 Wang, K., Zhang, Y., Yahya, K., Wu, S. Y., and Grell, G.: Implementation and initial application of new
788 chemistry-aerosol options in WRF/Chem for simulating secondary organic aerosols and aerosol indirect effects
789 for regional air quality, *Atmos. Environ.*, 115, 716–732, <https://doi.org/10.1016/j.atmosenv.2014.12.007>, 2015.

790 Wang, K., Hattori, S., Lin, M., Ishino, S., Alexander, B., Kamezaki, K., Yoshida, N., and Kang, S.: Isotopic
791 constraints on atmospheric sulfate formation pathways in the Mt. Everest region, southern Tibetan Plateau,
792 *Atmos. Chem. Phys.*, 21, 8357–8376, <https://doi.org/10.5194/acp-21-8357-2021>, 2021.

793 Wang, T., Li, S., Shen, Y., Deng, J., and Xie, M.: Investigations on direct and indirect effect of nitrate on
794 temperature and precipitation in China using a regional climate chemistry modeling system, *J. Geophys. Res.*
795 *Atmos.*, 115, 1–13, <https://doi.org/10.1029/2009JD013264>, 2010.

796 Wang, Y., Zheng, X., Dong, X., Xi, B., Wu, P., Logan, T., and Yung, Y. L.: Impacts of long-range transport of
797 aerosols on marine-boundary-layer clouds in the eastern North Atlantic, *Atmos. Chem. Phys.*, 20, 14741–14755,
798 <https://doi.org/10.5194/acp-20-14741-2020>, 2020.

799 Wang, Z., Xue, L., Liu, J., Ding, K., Lou, S., Ding, A., Wang, J., and Huang, X.: Roles of Atmospheric
800 Aerosols in Extreme Meteorological Events: a Systematic Review, *Curr. Pollut. Reports*, 8, 177–188,
801 <https://doi.org/10.1007/s40726-022-00216-9>, 2022.

802 Wiedinmyer, C., Akagi, S. K., Yokelson, R. J., and Emmons, L. K.: The Fire INventory from NCAR (FINN) – a
803 high resolution global model to estimate the emissions from open burning, *Geosci. Model Dev. Discuss.*, 3,
804 2439–2476, <https://doi.org/10.5194/gmdd-3-2439-2010>, 2010.

805 Yang, Q., Gustafson, W. I., Fast, J. D., Wang, H., Easter, R. C., Morrison, H., Lee, Y. N., Chapman, E. G.,
806 Spak, S. N., and Mena-Carrasco, M. A.: Assessing regional scale predictions of aerosols, marine stratocumulus,
807 and their interactions during VOCALS-REx using WRF-Chem, *Atmos. Chem. Phys.*, 11, 11951–11975,
808 <https://doi.org/10.5194/acp-11-11951-2011>, 2011.

809 Yu, F., Ma, X., and Luo, G.: Anthropogenic contribution to cloud condensation nuclei and the first aerosol
810 indirect climate effect, *Environ. Res. Lett.*, 8, <https://doi.org/10.1088/1748-9326/8/2/024029>, 2013.

811 Zaveri, R. A., Easter, R. C., Fast, J. D., and Peters, L. K.: Model for Simulating Aerosol Interactions and
812 Chemistry (MOSAIC), *J. Geophys. Res. Atmos.*, 113, 1–29, <https://doi.org/10.1029/2007JD008782>, 2008.

813 Zaveri, R. A., Easter, R. C., Singh, B., Wang, H., Lu, Z., Tilmes, S., Emmons, L. K., Vitt, F., Zhang, R., Liu, X.,
814 Ghan, S. J., and Rasch, P. J.: Development and Evaluation of Chemistry-Aerosol-Climate Model CAM5-Chem-
815 MAM7-MOSAIC: Global Atmospheric Distribution and Radiative Effects of Nitrate Aerosol, *J. Adv. Model.*
816 *Earth Syst.*, 13, 1–24, <https://doi.org/10.1029/2020MS002346>, 2021.

817 Zhang, Y., Wen, X. Y., and Jang, C. J.: Simulating chemistry-aerosol-cloud-radiation-climate feedbacks over
818 the continental U.S. using the online-coupled Weather Research Forecasting Model with chemistry
819 (WRF/Chem), *Atmos. Environ.*, 44, 3568–3582, <https://doi.org/10.1016/j.atmosenv.2010.05.056>, 2010.

820 Zhao, C., Liu, X., Leung, L. R., Johnson, B., McFarlane, S. A., Gustafson, W. I., Fast, J. D., and Easter, R.: The
821 spatial distribution of mineral dust and its shortwave radiative forcing over North Africa: Modeling sensitivities
822 to dust emissions and aerosol size treatments, *Atmos. Chem. Phys.*, 10, 8821–8838, <https://doi.org/10.5194/acp-10-8821-2010>, 2010.

824 Zhao, C., Liu, X., Leung, L. R., and Hagos, S.: Radiative impact of mineral dust on monsoon precipitation
825 variability over West Africa, *Atmos. Chem. Phys.*, 11, 1879–1893, <https://doi.org/10.5194/acp-11-1879-2011>,
826 2011.

827

828

829